AD-A175 838 OPTICALLY TUNED MILLIMETRE-WAVE CW IMPATT SOURCE(U) 1/1
MARCONI ELECTRONIC DEVICES LTD LINCOLN (ENGLAND)
J F SINGLETON ET AL APR 86 TR-85 DAJA45-84-C-0045
UNCLASSIFIED F/G 9/1 NL

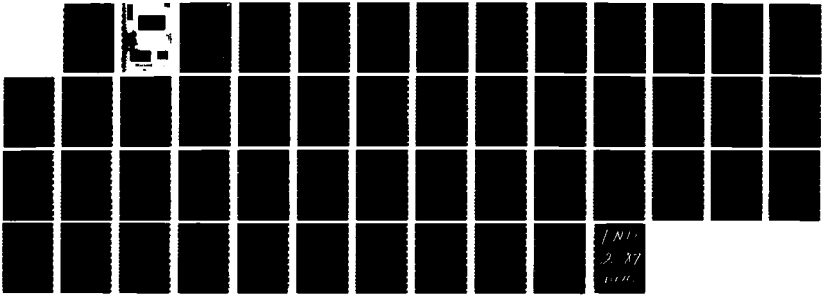

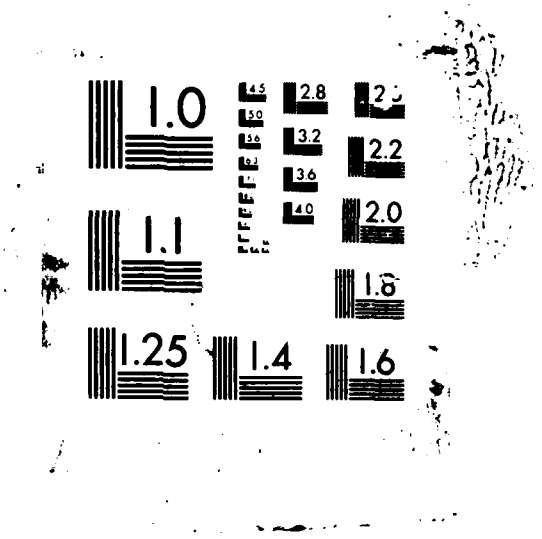
1.0
1.1
1.25
1.4
1.6
1.8
2.0
2.2
2.8
3.2
3.6
4.0

Contract No. DAJA 45-84-C-0045
Optically tuned mm-wave c.w.
IMPATT source

FINAL REPORT

TR85 April 1986

Marconi
Electronic Devices

(2)

Contract No. DAJA 45-84-C-0045
Optically tuned mm-wave c.w.
IMPATT source

FINAL REPORT

TR85 April 1986

Marconi Electronic Devices Ltd.,
Doddington Road,
Lincoln,
LN6 3LF,
U.K.

Dept. of Electrical and Electronic Eng.,
Queen Mary College,
Mile End Road,
London, E1 4NS,
U.K.

Prepared by:

Dr. J.F. Singleton, MEDL, Lincoln.
Miss S. Brunt, MEDL Lincoln
Dr. A.J. Seeds, QMC, London.

Distribution

Fiscal Officer (24 copies)	U.S. Army Research, Development and Standardization Group, London.
Dr. A. Seeds	Queen Mary College, London
Dr. J. Forrest	MDS Stanmore
Dr. J. Singleton	MEDL Lincoln
S. Brunt	" "
D.A. Williams	" "
S. Neylon	" "
E. Smith	" "
Dr. J. Ondria	" "

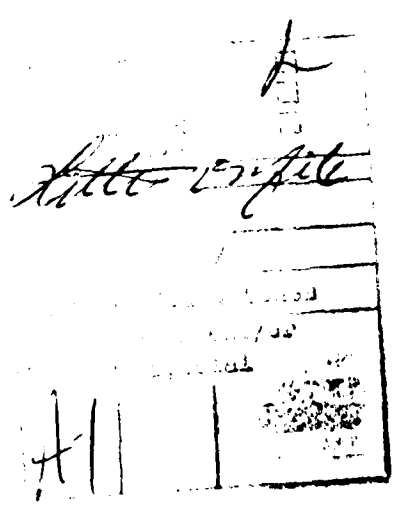

1. Contract Objectives

The main objective of the contract was to carry out a one year feasibility study on the use of an optical signal to control the operating frequency of a millimetre-wave IMPATT oscillator. The study involved a theoretical analysis of optical tuning in IMPATT diodes, computer modelling of optical tuning behaviour, including transient behaviour, and experimental measurements on a W-Band optically controlled oscillator.

2. Summary of Principal Results

An analytic theory of optical tuning in IMPATT oscillators has been developed, leading to a simple equation relating the change in oscillator frequency to the optically injected current. Major predictions of the equation are that the change in oscillator frequency is linearly proportional to the optically injected current that the proportionality constant varies as the reciprocal of the oscillator Q factor and that avalanche multiplication increases the optical tuning effect significantly at the higher oscillator voltage swings. It is predicted that a 5mW semiconductor laser would produce a tuning range of the order of 1% in a W-Band IMPATT oscillator having a Q of 200.

A comprehensive computer model of the optically tuned IMPATT oscillator has been developed. An important result obtained from this model is that optically generated electrons produce a considerably greater tuning effect than optically generated holes in a silicon IMPATT oscillator due to the unequal ionisation coefficients in silicon. The model has been used to produce an estimate of tuning speed in an optically controlled W-Band oscillator. For a low Q oscillator a 0.2% change in frequency was produced in 55ps which compares well with conventional tuning techniques.

Optical tuning was demonstrated experimentally in a W-Band IMPATT oscillator. Theoretical predictions of the optical tuning slope were verified. The maximum frequency change obtained was about 10MHz owing to the difficulty in coupling the light into a conventional IMPATT structure. Methods of improving the coupling efficiency are currently under investigation.

3. Introduction

Optical control techniques offer a number of advantages in microwave and millimetre-wave systems. First, the control port is electrically isolated from the active device. Second, high power devices, that are difficult to control by conventional means, such as IMPATT diodes, can be controlled. Third, control signals can be distributed using optical fibres and processed using electro-optic, acousto-optic or other techniques. A review of some of the systems aspects of optical control has been given by Kiehl (3.1).

A number of active devices have been successfully controlled using optical

signals. Yen and Barnoski (3.2) described switching of a bipolar transistor oscillator using a signal from a semiconductor laser. By modulating the laser drive current at a frequency close to a subharmonic of the oscillation frequency it was possible to lock this frequency to that of the modulation; this is known as optical injection locking.

Optical tuning of the oscillation frequency in MESFET oscillators has also been demonstrated (3.3) as has optical injection locking (3.4).

In two terminal devices, substantial optical tuning and power variation effects have been observed by Kiehl (3.5) in TRAPATT oscillators operating at frequencies of up to 1.5GHz.

Optical frequency tuning of IMPATT oscillators has been investigated by Chiu and Freyer (3.6) for an operating frequency of 8.7GHz. Seeds and Forrest (3.7) have also demonstrated optical injection locking of IMPATT oscillators.

Almost all of the optical control work carried out so far has used frequencies in or below X-Band, although optical enhancement or inhibition of oscillations in pulsed 70GHz IMPATT oscillators has been reported by Gerlach and Wellman (3.8). However, the potential systems applications of optical control are most attractive at millimetre-wave frequencies. The object of the present programme is to develop optical control techniques for W-Band IMPATT oscillators, including theoretical models for optical tuning, computer modelling studies and experimental work.

4. Theoretical Analysis of Optical Tuning in IMPATT Oscillators

4.1. IMPATT Diode Model

When the IMPATT diode is illuminated with light of photon energy greater than the gap energy of the material from which it is made, electron-hole pairs are generated in the device. These carriers produce a reverse saturation current which adds to that generated thermally, altering the timing of the avalanche cycle, and producing a change in oscillator operating frequency.

A general analysis of IMPATT diode operation is a difficult matter, particularly when the avalanche ionisation coefficients for electrons and holes are unequal. However a relatively straightforward solution is possible if the ionisation coefficients are assumed to be equal, leading to Read's equation (4.1):

$$\frac{\tau_a}{2}\frac{dJ}{dt} = J\left[\int_0^{L_a} \alpha\, dz - 1\right] + J_s \qquad \ldots\ldots 4.1$$

where J is the particle current density in the avalanche zone of length L_a, τ_a is the avalanche zone transit time, α is the avalanche

ionisation coefficient and J_s the total reverse saturation current density. Inherent in this equation is the assumption of an avalanche zone of constant length and defined transit time. For the optical tuning analysis, the reverse saturation current is assumed to be of the form

$$J_s = J_{so} + J_{st} \qquad \ldots.4.2$$

where J_{so} is the optically generated current density and J_{st} the thermally generated current density.

To solve equation 4.1, an expression for the electric field dependence of the ionisation coefficient, α , is required. A useful model is

$$\alpha = \alpha_o \left(\frac{E}{E_o}\right)^m \qquad \ldots\ldots.4.3$$

where E is the electric field, m is an ionisation non-linearity constant ($m \simeq 6$ for silicon) and α_o and E_o are constants. Note that this equation neglects the saturation in ionisation coefficients at high electric fields.

If the doping of the avalanche zone is uniform and space charge effects are neglected, the field in an abrupt junction diode will vary from its peak value, E_p, down to the highest value in the drift zone, E_d, with constant dE/dz . Evaluation of the ionisation integral is then simple giving

$$\int_o^{L_a} \alpha \, dz = \left(\frac{E_p}{E_{po}}\right)^{(m+1)} \qquad \ldots\ldots.4.4$$

where E_{po} is the peak field at breakdown and it is assumed that $E_d << E_p$.

Assuming the diode to be embedded in a resonant cavity of moderately high Q factor, the voltage variation across the diode will be near sinusoidal. The peak electric field can then be written

$$E_p = E_{po} - E_b + E_1 \sin(\omega t + \delta) \qquad \ldots4.5$$

for a diode terminal voltage

$$v = V_{po} + L(E_1 \sin \omega t - E_b) \qquad \ldots4.6$$

Here E_b is a back bias field resulting from the combined effects of ionisation non-linearity, reverse saturation current and carrier space charge, E_1 is the peak value of the modulated component of electric field, ω the operating frequency, L the total depletion width and V_{po} the breakdown voltage. Note that equation 4.6 is only valid providing the diode remains punched-through over the complete r.f. cycle. In equation 4.5. the phase angle between the voltage applied to the diode

and the a.c. component of the avalanche zone field is used to take account of back bias and space charge effects: details of its evaluation are given by Carroll (4.2)

Substituting equations 4.5 and 4.4. into equation 4.1.

$$\frac{dJ}{dt} = \frac{2J}{\tau_a}\left[\left(1 - \frac{E_b}{E_{po}} + \frac{E_1}{E_{po}}\sin(\omega t + \delta)\right)^{m+1} - 1\right] + \frac{2J_s}{\tau_a} \qquad \ldots\ldots\ldots 4.7$$

Under normal operation E_b, $E_1 << E_{po}$ so that the inner bracket term can be expanded using the Taylor approximation, yielding

$$\frac{dJ}{dt} = \frac{2(m+1)}{\tau_a} J\left[\frac{m}{4}\left(\frac{E_1}{E_{po}}\right)^2 - \frac{E_b}{E_{po}} + \frac{E_1}{E_{po}}\sin(\omega t + \delta)\right] + \frac{2J_s}{\tau_a} \qquad \ldots\ldots\ldots 4.8$$

where harmonic terms have been neglected.

Equation 4.8 is a linear first order equation and can be solved using an integrating factor expanded in terms of modified Bessel functions to give a simple expression for the fundamental component of the conduction current.

$$J_1 = -2\left[J_{dc}\frac{I_1\{X\}}{I_o\{X\}}\cos(\omega t + \delta_s)\right] \qquad \ldots\ldots\ldots 4.9$$

where J_{dc} is the IMPATT bias current density and δ_s is a modified phase angle

$$\delta_s = \delta + \sin^{-1}\left(\frac{J_s}{J_{dc}}\frac{2I_o^2\{X\} - 3I_o\{X\}I_2\{X\}}{\omega\tau_a}\right) \qquad \ldots\ldots\ldots 4.10$$

where $I_n\{X\}$ are modified Bessel function coefficients of order n and argument

$$X = \frac{2(m+1)E_1}{\omega\tau_a E_{po}} \qquad \ldots\ldots\ldots 4.11$$

In deriving equation 4.9, it has been assumed that $J_s << J_{dc}$ and also that Bessel function terms of order greater than 2 can be neglected. These assumptions apply providing the voltage swing across the diode is moderate and the optically injected current is small

The effect of the drift zone can be modelled using the Ramo-Shockley theorem assuming that all carrier motion is at saturated velocity, v_s, and that the drift zone is of constant length L_d, giving the terminal conduction current as

$$J_{t1} = -2 J_{dc} \frac{\sin\left(\frac{\omega\tau_d}{2}\right)}{\left(\frac{\omega\tau_d}{2}\right)} \frac{I_1\{X\}}{I_o\{X\}} \cos\left(\omega\left(t-\frac{\tau_d}{2}\right) + \delta_s\right) \quad \ldots\ldots 4.12$$

where τ_d ($= L_d / v_s$) is the drift zone transit time.

The diode admittance can now be obtained by dividing by the applied a.c. voltage, v_1 and adding the depletion susceptance, ωC_d. From equation 4.6

$$v_1 = -j V_1 \exp j\omega t \quad \ldots\ldots 4.13$$

where V_1 is the peak value of the fundamental component of the diode terminal voltage. Thus the diode admittance Y_1 ($= G_1 + jB_1$) is found from

$$G_1 = \frac{-2I_{dc}}{V_1} \frac{\sin\left(\frac{\omega\tau_d}{2}\right)}{\left(\frac{\omega\tau_d}{2}\right)} \frac{I_1\{X\}}{I_o\{X\}} \sin\left(\frac{\omega\tau_d}{2} - \delta_s\right) \quad \ldots\ldots 4.14$$

and

$$B_1 = \frac{-2I_{dc}}{V_1} \frac{\sin\left(\frac{\omega\tau_d}{2}\right)}{\left(\frac{\omega\tau_d}{2}\right)} \frac{I_1\{X\}}{I_o\{X\}} \cos\left(\frac{\omega\tau_d}{2} - \delta_s\right) + \omega C_d \quad \ldots\ldots 4.15$$

where I_{dc} is the diode bias current.

Optical tuning results from the reverse saturation current dependence of δ_s in the above equations.

4.2 Oscillator Circuit Model

To obtain optical tuning predictions, a circuit model for the oscillator is required. A simple lumped model is shown in Figure 4.1.

For stable oscillation

$$G_1 + G_L = 0 \quad \text{....4.16}$$

$$B_1 + B_L = 0 \quad \text{....4.17}$$

Thus, from equations 4.14 and 4.15

$$G_L = \frac{2I_{dc} \sin\left(\frac{\omega\tau_d}{2}\right) I_1\{X\}}{V_1 \left(\frac{\omega\tau_d}{2}\right) I_o\{X\}} \sin\left(\frac{\omega\tau_d}{2} - \delta_s\right) \quad \text{.....4.18}$$

and

$$B_L = \frac{2I_{dc} \sin\left(\frac{\omega\tau_d}{2}\right) I_1\{X\}}{V_1 \left(\frac{\omega\tau_d}{2}\right) I_o\{X\}} \cos\left(\frac{\omega\tau_d}{2} - \delta_s\right) - \omega C_d \quad \text{.....4.19}$$

Dividing equation 4.19 by equation 4.18 and defining B_L by $B_L = -1/(\omega L_L)$ gives

$$\omega C_d - \frac{1}{\omega L_L} = G_L \cot\left(\frac{\omega\tau_d}{2} - \delta_s\right) \quad \text{.....4.20}$$

An estimate of the tuning sensitivity can be obtained by assuming that $\omega = \omega_o + \Delta\omega$, where $\omega_o = (L_L C_d)^{-\frac{1}{2}}$ and that

$$\omega\tau_d \simeq \pi \quad \text{and} \quad \delta_s \ll \frac{\pi}{2} \quad \text{.....4.21}$$

These assumptions are valid for operation close to the frequency of zero active susceptance, at moderate signal levels so that back bias and space charge effects are small, and for low values of injected saturation currents. Equation 4.20 then becomes

$$2\Delta\omega C_d \simeq G_L \delta_s \quad \text{.....4.22}$$

From equation 4.10, with small injected saturation currents

$$\Delta\omega \sim \frac{G_L}{2C_d}\left[\delta + \frac{I_s}{I_{dc}}\frac{2\,I_o'\{X\} - 3I_o\{X\}\,I_2\{X\}}{\omega_o\ \tau_a}\right] \qquad \ldots\ldots.4.23$$

where I_s is the saturation current. The frequency shift with optically injected current, I_{so} is thus

$$\frac{d(\Delta f)}{dI_{so}} = \frac{G_L}{4\pi C_d I_{dc}}\frac{2\,I_o^2\{X\} - 3\,I_o\{X\}\ I_2\{X\}}{\omega_o\ \tau_a} \qquad \ldots\ldots.4.24$$

Defining oscillator Q factor as

$$Q = \frac{\omega_o\ C_d}{G_L} \qquad \ldots\ldots.4.25$$

one can rewrite equation 4.24 as

$$\frac{d(\Delta f)}{dI_{so}} = \frac{F_a\{X\}}{2\pi Q I_{dc}\tau_a} \qquad \ldots\ldots.4.26$$

where $F_a\{X\}$ is an avalanche gain factor

$$F_a\{X\} = \frac{2\,I_o^2\{X\} - 3\,I_o\{X\}\ I_2\{X\}}{2} \qquad \ldots\ldots.4.27$$

$F_a\{X\}$ is a strong function of voltage swing due to the Bessel function argument dependence on peak modulated electric field, equation 4.11. Figure 4.2 shows the variation of $F_a\{X\}$ with X. At low signal levels, the gain tends to unity but as the voltage swing increases the gain increases rapidly, thus enhancing the optical tuning effect. This avalanche gain factor considerably increases the attraction of the IMPATT as a device for optical control.

4.3. Optical Tuning Predictions

It is instructive at this stage to estimate the optical tuning range that can be achieved with a typical IMPATT oscillator.

The first requirement for this is a relation between the optically generated current I_{so} and the incident optical power, P_{op}. Assuming that each absorbed photon generates one hole-electron pair one obtains

$$I_{so} = \frac{\eta_{qe} e \lambda P_{op}}{hc} \qquad \ldots\ldots\ldots 4.28$$

where η_{qe} is the external quantum efficiency including reflection losses and spill-over, λ is the wavelength of the incident light, e is the electronic charge, h is Planck's constant and c is the velocity of light in vacuo. For an incident wavelength of 850nm and $\eta_{qe} = 1.0$ $I_{so}/P_{op} = 0.68$ A W^{-1}.

A typical IMPATT diode might have $L_a = 0.2L_d$, which with the condition on τ_d, approximations 4.21, gives $\tau_a = 0.2\pi/\omega_o$. With a typical voltage swing of $E_1/E_{po} = 0.2$ equation 4.11 gives $X \simeq 4.5$ and thus from Figure 4.2 $F_a\{X\} = 26.5$. The tuning slope can now be obtained from equation 4.26. Consider a W-Band oscillator with f_o (= $\omega_o/2\pi$) = 100GHz, I_{dc} = 100mA and Q = 200. Then $d(\Delta f)/dI_{so}$ = 210GHz A^{-1}. A typical semiconductor laser having an output power of 5mW at 850nm would then give a tuning range of 714MHz or about 0.7%.

The calculation above assumes an external quantum efficiency of unity. It will be seen that with normal IMPATT structures, the efficiency is much less than this value thereby reducing the tuning range. An important area for future work will be to investigate ways of improving this parameter.

Equation 4.26 also shows that the tuning range is increased by reducing the oscillator Q. Obviously this approach has to be tempered with regard for other systems requirements such as oscillator noise.

Finally reducing the bias current has a complicated effect since whilst there is an I_{dc}^{-1} dependence in equation 4.26, this is more than compensated by the effect of the reduced voltage swing with reduced bias current except at very low biases where the $F_a\{Y\}$ slope is less.

4.4. Conclusion

An analytic theory for optical tuning of IMPATT diode oscillators has been developed. It predicts tuning ranges of the order of 1% in typical W-Band oscillators with optical powers of a few milliwatts. The theory is related to parameters of the device and circuit which are relatively straightforward to determine.

5. Computer Modelling Studies

5.1. Description of the Model

As can be seen from the previous section, a number of approximations are required to permit the derivation of an analytic expression for the optical tuning range of an IMPATT oscillator. Of particular importance is the assumption of equal ionisation coefficients for electrons and holes. In silicon the coefficient for electrons is an order of magnitude greater than that for holes, over a wide range of electric field. The optical tuning behaviour is thus considerably dependent on the composition of the optically generated current, and hence on the illumination configuration. A computer model has therefore been used to examine these effects and also to evaluate transient tuning performance.

The model used, known as the Full Simulation Suite (FSS), comprises three linked programs. In the d.c. Program (DCP) all time variations are made zero so that the d.c. characteristics of the device can be examined. An output file comprising electric field and carried density profiles within the diode is produced and used as input data for the Small Signal Program (SSP) and the Full Simulation Program (FSP).

The SSP uses perturbation methods to obtain the small signal admittance of the IMPATT as a function of frequency. The FSP is a comprehensive large signal model for avalanche diodes based on the solution of the following equations in one spatial dimension and time

$$J_n = e\, n\, v_n - e\, D_n \frac{\partial n}{\partial z} \qquad \text{.....5.1}$$

$$J_p = e\, p\, v_p + e\, D_p \frac{\partial p}{\partial z} \qquad \text{.....5.2}$$

$$\frac{\partial n}{\partial t} = -\frac{1}{e}\frac{\partial J_n}{\partial z} + g_n \qquad \text{.....5.3}$$

$$\frac{\partial p}{\partial t} = \frac{1}{e}\frac{\partial J_p}{\partial z} + g_p \qquad \text{.....5.4}$$

$$\frac{\partial E}{\partial z} = \frac{-\rho}{\varepsilon_r \varepsilon_o} \qquad \text{.....5.5}$$

where J is the current density, n the free electron density, p the free hole density, v the carrier velocity, D the diffusion coefficient, g the carrier generation rate, E the electric field strength, ρ the free charge density, ε_o the primary electric constant, ε_r the relative permittivity, e the electronic charge, and z and t the spatial and temporal dimensions. The subscripts n and p denote free electrons and free holes respectively. Equations 5.1 and 5.2 are approximate representations of Boltzmann's transport equation, equations 5.3 and 5.4 are continuity equations for

electrons and holes, while equation 5.5 is the differential form of Gauss' theorem. Equations 5.1 to 5.5 use a sign convention in which the electron velocity is directed oppositely to the electron motion, a convention commonly adopted in analyses of Gunn devices.

The effect of optical carrier generation is introduced through the generation term in equations 5.3 and 5.4

$$g_n = g_p = \frac{1}{e}\left[\alpha_n J_n + \alpha_p J_p\right] + \gamma S + \Theta \qquad \ldots\ldots.5.6$$

Here, the α terms represent avalanche generation , the γ term optical carrier generation resulting from illumination with light of intensity S and the Θ term thermal carrier generation. Note that γ is spatially variant owing to optical absorption in the IMPATT material.

The numerical techniques used in the solution of equations 5.1 to 5.5. are described by Blakey et al (5.1) while the method of modelling optical carrier generation is detailed by Seeds (5.2). The use of the drift-diffusion approximation and the representation of carrier velocities and avalanche ionisation coefficients as instantaneious function of electric field limit the usefulness of the model at the higher millimetre wave frequencies. However, work done by Blakey et al to compare the predictions of the model with those obtained from an energy and momentum conserving model (5.3) has shown that for silicon IMPATTs the error introduced at W-Band is less than that caused by uncertainty in the material parameters.

5.2. Material Parameters and Doping Profile

Carrier velocity/field characteristics were fitted to the measured values of Duh and Moll (5.4) for saturated electron velocity toegther with the temperature dependence of carrier mobility given by Sze (5.5). The temperature dependence of the avalanche ionisation coefficients was based on the model of Crowell and Sze (5.6). A junction temperature of 450K was assumed throughout the modelling work.

The measured doping profile for the devices used in the experimental programme is shown in Figure 5.1. A complimentary error function model for the doping profile was used in the modelling work.

$$N = N_e + 0.5\,(N_d - N_e)\,\mathrm{erfc}\left(\frac{W - z}{W_d}\right) - N_a\,\mathrm{erfc}\left(\frac{z}{W_a}\right) \qquad \ldots\ldots.5.7$$

where N is the doping density (positive for N-type material). The epitaxial layer is of width W and doping density N_e. N_d is the substrate doping density and N_a is the surface acceptor doping concentration. W_a determines the junction depth and W_d characterises the substrate out-diffusion similarly. The following values were used:

N_e = 1.40×10^{17} cm^{-3}

N_d = 2.80×10^{19} cm^{-3}

N_a = 1.50×10^{20} cm^{-3}

W = 6.10×10^{-5} cm

W_d = 3.10×10^{-6} cm

W_a = 1.00×10^{-5} cm

Figure 5.2 shows the modelled profile; it can be seen to match the measured profile, Figure 5.1. quite closely.

5.3. DCP Results

A bias current density of 2.45×10^4A cm^{-2} was used for the modelling work, corresponding to a bias current of 120mA in the experimental devices. Figure 5.3. shows the electric field and electron current density profiles for the device. The diode is seen to be just punched-through, so that losses in undepleted epitaxial material would be expected to be small.

An estimate of the avalanche zone length, L_a, required for the theory of Section 4, can be obtained from the electron current density curve. Using a 20% - 80% criterion gives the length as 0.07 μm.

The predicted bias voltage was 11.9V with the diode not oscillating. In comparing this value with experimental results it has to be remembered that the DCP neglects voltage drops in undepleted material, contacts and bias circuitry.

5.4. SSP Results

The SSP was used to investigate the effect of the composition of optically injected current on the diode admittance. An operating frequency of 94GHz was selected to approximate the values used experimentally.

Figure 5.4. shows the admittance values obtained, with injected current density as the parameter. The maximum injected current density shown, 80Acm^{-2}, would correspond to that obtainable with illumination from a 0.6mW, 850nm, optical source, assuming an external quantum efficiency of unity.

Electron injection is seen to have considerably greater effect than hole injection. This is a consequence of the higher avalanche ionisation coefficient for electrons in silicon. Clearly it is desirable to maximise electron injection in optical control. This can be achieved by

illuminating the diode from the P^+ region.

5.5. FSP Results

The large signal admittance of the diode was determined at a frequency of 94GHz for 25% sinusoidal voltage modulation. Figure 5.5 shows the equivalent circuit used and a detailed explanation of its operation is given in (5.1). C_p was selected as 4.00pF and R_p as 1.0 Ω. The output obtained is shown in Figure 5.6. The modelled efficiency was 3.6%, a typical value for a W-Band, single drift silicon device. Unlike the DCP, the FSP models undepleted epitaxial material. For this reason the bias voltage obtained with the FSP is higher than that with the DCP at the same current density.

In order to model optical tuning characteristics with the FSP the IMPATT diode must be connected to a suitable oscillator circuit. Figure 5.7 shows a simple arrangement. L_p represents the diode bond wire inductance, R_p the diode parasitic resistance, R_L the load resistance, C the d.c. block capacitance and Z_t a quarter-wave transformer. If L_p is selected to resonate with the capacitive susceptance of the diode the impedance seen looking towards the diode at plane X-X' is real and negative. The amplitude of the oscillation is then determined by selecting Z_t to match R_L to the impedance at X-X' for the required operating point.

To match the experimental conditions the circuit was designed to operate at about 94GHz with between 20 and 30% voltage modulation, for a bias current of 140mA. This required the following circuit values:

$R_p = 1.0\Omega$

$L_p = 0.045nH$

$C = 4.00pF$

$Z_t = 30\Omega$

$R_L = 50\Omega$

Figure 5.8 shows the modelled growth of oscillation from switch on. With a thermally generated saturation current density of 0.32A cm^{-2} and no optically generated current, the oscillation stabilised at a frequency of 94.195GHz with 23% voltage modulation.

Opitcal tuning was investigated for two illumination configurations. In the first, electrons were injected into the depletion zone from the P^+ region whereas in the second holes were injected from the N^+ region. These configurations correspond to illumination from opposite ends of the IMPATT structure. Figure 5.9 shows the optical tuning characteristics obtained for optically injected current densities of up to 2A cm^{-2}

corresponding to 10μ A in an experimental device. The change in frequency with injected current is linear, in accordance with the predictions of equation 4.26. Substituting values for the model used gives a tuning slope of 8.8MHz μA^{-1}, which has been plotted as a solid line in Figure 5.9. The computer modelling results for electron and hole tuning lie above and below this line respectively. This is because the analytic theory assumes that the avalanche ionisation coefficients for electrons and holes are equal whereas in fact those for electrons are much greater than those for holes. Electron injection therefore produces a much greater tuning effect than hole injection. With this restriction, agreement between the theory of Section 4 and the modelling studies is good.

The tuning slope of the modelled oscillator is much larger than that estimated for a typical experimental oscillator in Section 4. This is because the modelled oscillator has a Q of 1.6 which is much lower than most practical oscillators.

The FSP can be used to investigate transient effects and Figure 5.10 shows the tuning transient resulting from a step change in optically injected electron current from 0 to 2 A cm^{-2}. 90% of the frequency change was achieved in 55ps. This compares very favourably with the speed of conventional electronic tuning techniques such as varactor tuning and may afford novel systems possibilities.

5.6. Conclusion

A suite of computer programs for modelling optical tuning effects in IMPATT oscillators has been described. For silicon IMPATTs it has been shown that electron injection produces considerably greater tuning effects than hole injection. This has important implications for the design of optically controlled IMPATT structures. It has also been shown that optical tuning can produce very rapid frequency changes, a result of considerable systems interest.

6. Experimental Work

6.1. Devices, Packaging and Oscillator Design

The devices used were single drift silicon IMPATTs having a doping profile similar to that shown in Figure 5.1. These were mounted in quartz ring packages, as shown in Figure 6.1.

The oscillator circuit used was the well known resonant cap design (6.1), shown in Figure 6.2.

Figure 6.3 shows the measured r.f. output power as a function of bias current. For a current of 120mA the efficiency was 3.1% which is in good agreement with the computer model result of 3.6% (see Section 5.5) bearing in mind that the computer model neglects circuit losses

6.2. Initial Work

Initial experiments were carried out using a He-Ne laser emitting at 632.8nm. Light from this was shone into the cavity so as to be incident on the side of the diode, parallel to the plane of the junction. The optically generated reverse saturation current was measured at a reverse bias voltage of 6V. The maximum value obtained was 2 μA. An estimate of the optical power incident on the device was made by comparing the relative cross-sections of the laser beam and the illuminated diode area. Substituting in equation 4.28 gave a value of 1.5 μA for the reverse saturation current, showing reasonable agreement with the measured result.

When the diode was illuminated a small, but distinct, frequency shift of 200-300kHz was observed on the spectrum analyser monitoring the oscillator output.

The oscillator Q was measured approximately by the load-pull method as 160, and this value was used to predict the optical tuning range from equations 4.26 and 4.27. From the computer modelling work of Section 5.3 τ_a was estimated to be 0.7ps, which gives a tuning slope of 120 kHz μA^{-1} for a free-running frequency of 95GHz with 10% voltage modulation at a bias current of 120mA. This is in good agreement with the measured result.

6.3. Tuning Characteristics with Semiconductor Laser Source

Initial work with the He-Ne laser system had successfully demonstrated optical tuning of a W-Band oscillator and the frequency shift was in accord with theoretical predictions. However, use of the He-Ne laser had three significant disadvantages. Firstly, the room temperature absorption length in silicon is 2.0 m at a wavelength of 632.8nm (6.2). The mesa diameter of the IMPATT diodes used was 25 μm. Thus illumination in the plane of the junction was seriously non-uniform. Secondly, the output power of the laser could not be varied without the introduction of external optical components which would be likely to introduce beam steering difficulties. Finally a He-Ne laser would be bulky and inconvenient in systems applications. For these reasons further experimental work was based on the use of semiconductor lasers.

The laser type selected was the STC LC30-19, a GaAs/GaAlAs double heterostructure, stripe geometry device, emitting at 850nm. At this wavelength the optical absorption length in silicon is 11 μm, a value more suitable for the illumination geometry employed.

The laser was supplied with an optical fibre tail output of 50/125μm graded index fibre. The fibre was coupled to the active device through a small hole in the oscillator cavity wall with the fibre position optimised using a micromanipulator. Figure 6.4 shows the configuration

used in detail.

Control of the laser temperature was by a Peltier cooler within the laser package in conjunction with an external control circuit. A monitor photodiode was also present in the package, enabling the laser output power to be determined following an initial calibration run.

Using this arrangement optically generated reverse saturation currents of up to 20.5μA were obtained for an optical power, measured at the fibre end, of 3mW. From equation 4.28 this result implies an external quantum efficiency of 1.1%. This low value is due partly to refraction in the quartz ring package and partly to the small height of the IMPATT structure ($\approx 3\mu$m total) relative to the fibre core diameter of 50μm.

Although the coupling efficiency was poor, it was considerably higher than that obtained in the initial work and the tuning ranges were therefore correspondingly greater. Figure 6.5 shows a typical spectrum analyser display for an oscillator bias current of 100mA, giving a free running frequency of 91.83GHz. The centre peak is the output of the unilluminated oscillator, while the right-hand peak is the output of the oscillator with an optically generated current of 20.3μA. The frequency shift obtained was 9.4MHz.

Figure 6.6 is a plot of oscillation frequency shift against optically generated current. The shift is proportional to current, as predicted by equation 4.23. This linear dependency was confirmed for a number of different IMPATT diodes at various bias currents, Figure 6.7.

The measured tuning slopes can be compared with theory if the Q of the oscillator and the operating conditions are known. For this comparison the Q of a particular oscillator was measured by injection locking. Figure 6.8 shows the experimental arrangement used. From measurements of the injected power, the oscillator output power and the locking range the Q was determined, using equation A.1.12 of Appendix 1, as 204. Figure 6.9 shows the measured optical tuning characteristic for a bias current of 120mA. From the graph $d(\Delta f)/dI_{S0} = 225\text{kHz}\,\mu\text{A}^{-1}$.

From the measured output power $F_a\{X\}$ was estimated to be 27, giving a calculated tuning slope of $253\text{kHz}\,\mu\text{A}^{-1}$ from equation 4.26. Thus agreement is reasonable, particularly bearing in mind that the theory assumes equal avalanche ionisation coefficients for holes and electrons.

6.4. Conclusion

Optical tuning has been demonstrated for a W-Band IMPATT oscillator. The maximum frequency shift obtained was 9.4MHz using a 3mW semiconductor laser, however the coupling between the laser and the IMPATT was poor resulting in a low external quantum efficiency of 1.1%. If this could be improved to 65%, a value typical of high speed photodiodes, the tuning range should increase to over 600MHz, which

would be useful in systems applications.

The change in operating frequency with optically injected current was found to be linear in accordance with the predictions of Section 4. Comparison with the theoretical model gave reasonable agreement in the value of the tuning slope.

7. Conclusions and Suggestions for Further Work

7.1. Theory

A simple analytic theory for optical frequency tuning was developed in Section 4. it gives results in good agreement with both the computer model of Section 5 and the measured results of Section 6. Now that clearly measurable optical tuning effects are being obtained experimentally it will be possible to make a detailed comparison with the theory over a range of circuit and operating parameters.

A useful development of the theory would be to include further terms in the truncated Bessel function series to improve the accuracy at higher voltage swings. However the main sources of inaccuracy will remain the uncertainty in the values of device parameters and the limitation inherent in the equal ionisation coefficients assumption.

7.2. Computer Modelling

A comprehensive computer model of optical control effects in IMPATT diodes was presented in Section 5. When used to model the device structure selected for the experimental work, good agreement was obtained between measured and predicted values of d.c. characteristics and oscillator efficiency.

Use of the computer model enables the limitations of the equal ionisation coefficients assumption, used in the analytic theory, to be explored. For silicon, where the coefficient for electrons is much higher than that for holes, it was demonstrated that electron injection gives a considerably greater tuning effect than hole injection. This result has important implications for the design of an IMPATT structure for optical control.

An initial investigation of the tuning speed of optical control showed that very fast tuning was possible. This may have important systems applications. One would expect the Q of the oscillator to be the fundamental limitation. Further work needs to be done to investigate the effect of the oscillator circuit on tuning speed.

It has not so far been possible to model the oscillator circuit used experimentally due to its complexity. The main area for further work will be to develop a circuit model that will allow direct comparison with experiment.

7.3. Experimental Work

In Section 6, optical tuning of a W-Band IMPATT oscillator has been demonstrated experimentally. The tuning range obtained was small owing to difficulty in coupling the light into the IMPATT structure. Nevertheless the results have enabled the predictions of the analytic theory of Section 4 to be verified. Probably the most important area for future work is the development of IMPATT structures offering improved external quantum efficiency. Work is already under way to replace the quartz ring package, which introduces refraction and absorption losses with a package based on quartz stand-offs. Consideration is also being given to novel IMPATT fabrication techniques aimed at improving the coupling efficiency.

Other areas for future work are to carry out an experimental study of the tuning speed capabilities of optically controlled IMPATT oscillators and to investigate the effect of illumination on oscillator noise.

8. References

3.1 Kiehl, R.A.: 'Novel optical control techniques for solid-state radar transmitters', IEEE Trans., 1980, MTT-28, pp.409-413.

3.2 Yen, H.W. and Barnoski, M.K.: 'Optical injection locking and switching of transistor oscillators', Appl. Phys. Lett., 1978, 32, pp 182-184.

3.3 Sun, H.J., Gutmann, R.J. and Borrego, J.M.: 'D.C. and pulse-light illuminated optical responses of microwave GaAs-MESFET oscillators' Proc. IEE, 1984, 131I, pp. 31-37.

3.4 Salles, A.A. and Forrest, J.R.: 'Initial observations of optical injection locking of GaAs metal semiconductor field effect transistor oscillators', Appl. Phys. Lett., 1981, 38, pp.392-394.

3.5 Kiehl, R.A.: 'Behaviour and dynamics of optically controlled TRAPATT oscillators', Trans. IEEE, 1978, ED-25, pp.703-710.

3.6 Chiu, C. and Freyer, J.: 'Frquency modulation of IMPATT diodes by optical illumination', Proc. IEE, 1984, 131I, pp.28-30.

3.7 Seeds, A.J. and Forrest, J.R.: 'Initial observations of optical injection locking of an X-Band IMPATT oscillator', Electron Lett., 1978, 14, pp. 829-830.

3.8 Gerlach, H.W.A. and Wellman, R.: 'The behaviour of a pulsed millimetre-wave (70GHz) IMPATT diode oscillator during laser illumination', IEEE MTT Conf. Proc. 1981, pp. 70-72.

4.1 Read, W.T.: 'A proposed high-frequency negative resistance diode', Bell Syst. Tech. J., 1958, 37, pp.401-446.

4.2 Carroll, J.E.: 'Hot electron microwave generators', (Arnold, London, 1970), pp.197-212.

5.1 Blakey, P.A., Giblin, R.A. and Seeds, A.J.: 'Large-signal time-domain modelling of avalanche diodes', Trans. IEEE, 1979, ED-26, pp.1718-1728.

5.2 Seeds, A.J.: 'Time-domain computer modelling of opto-avalanche devices', IEE Colloquium on CAD of Microwave Electron Devices with Time-Varying Fields, 1983, Colloquium Digest 1983/69, pp.2/1-2/6.

5.3 Blakey, P.A., Froelich, R.K., Grondin, R.O. Mains, R.K. and Haddad, G.I.: 'Millimetre wave IMPATT diode modelling', Proc. Eighth Biennial Cornell Elec. Eng. Conf. 1981, pp.361-369.

5.4 Duh, C.Y. and Moll, J.L.: 'Temperature dependence of hot electron drift velocity in silicon at high electric field', Solid State Electron., 1968, 11, pp.917-932.

5.5 Sze, S.M.: 'Physics of semiconductor devices', (Wiley, New York, 1981), P.29.

5.6 Crowell, C.R. and Sze, S.M.: 'Temperature dependence of avalanche multiplication in semiconductors' Appl. Phys. Lett., 1966, 9, pp.242-244.

6.1 Misawa, T. and Kenyon, N.D.: 'An oscillator circuit with cap structure for millimetre-wave IMPATT diodes', Trans. IEEE, 1970, MTT-18, p.969.

6.2 Sze, S.M.: 'Physics of Semiconductor Devices', (Wiley, New York, 1981), p.42.

9. Publications

1. Singleton, J F., Seeds, A.J. and Brunt, S.P.: 'Optical control of W-Band IMPATT oscillators', presented at the IEE Colloquium on Optical Control and Generation of Microwave Signals, London, January 1986, and published in Colloquium Digest 1986/4, 5 pp.

10. Participating Personnel

Dr. J.R. Forrest,	Technical Director, Marconi Defence Systems, Stanmore (Technical Adviser)
Dr. A.J. Seeds	Lecturer, Queen Mary College, University of London (Consultant)
Dr. J.F. Singleton	Marconi Electronic Devices Ltd., Lincoln.
Miss. S.P. Brunt	Marconi Electronic Devices Ltd., Lincoln.
Mr. D.A. Williams	Marconi Electronic Devices Ltd., Lincoln (Programme Manager)

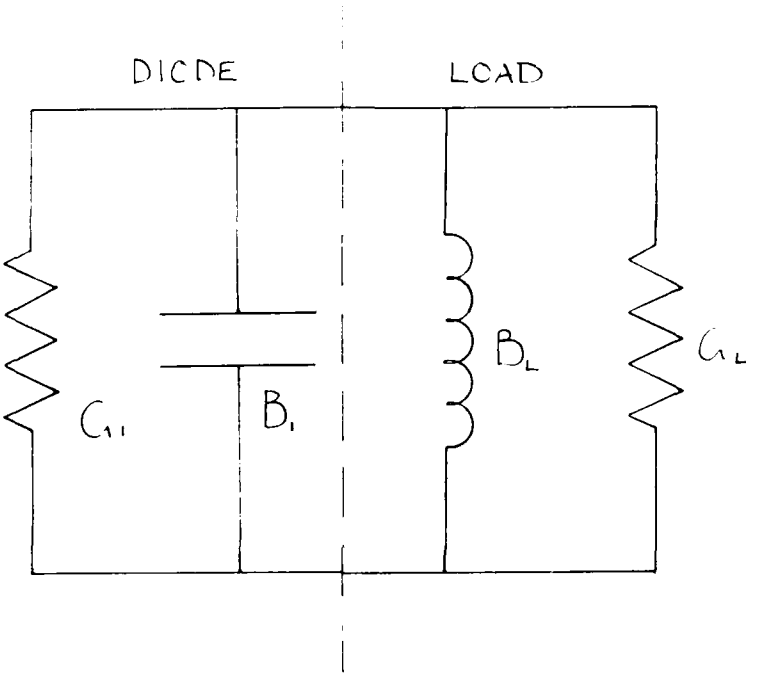

Figure 4.1 : Oscillator circuit model

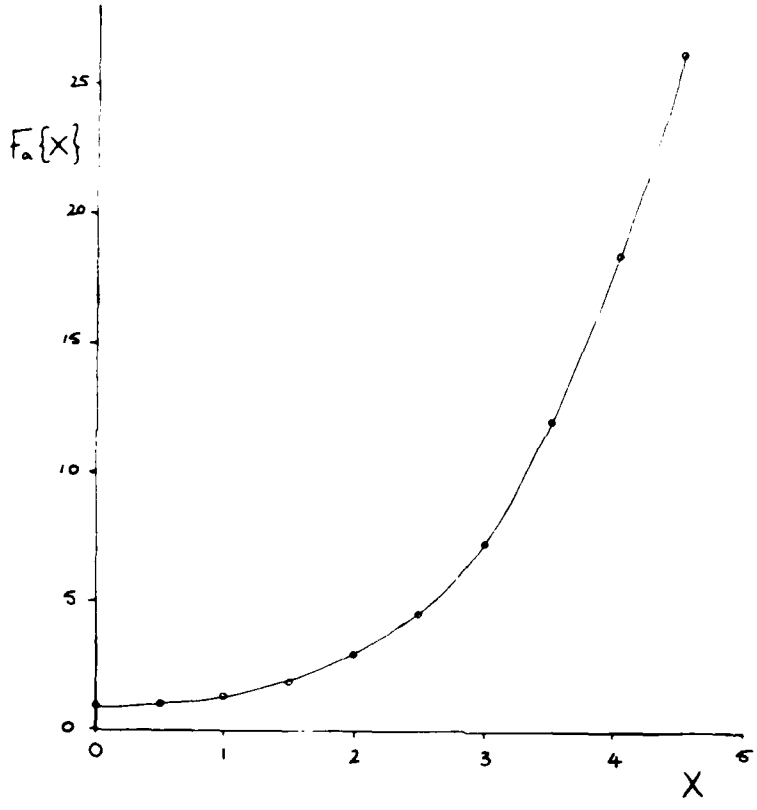

Figure 4.2 : Variation of avalanche gain parameter $F_a\{X\}$ with X.

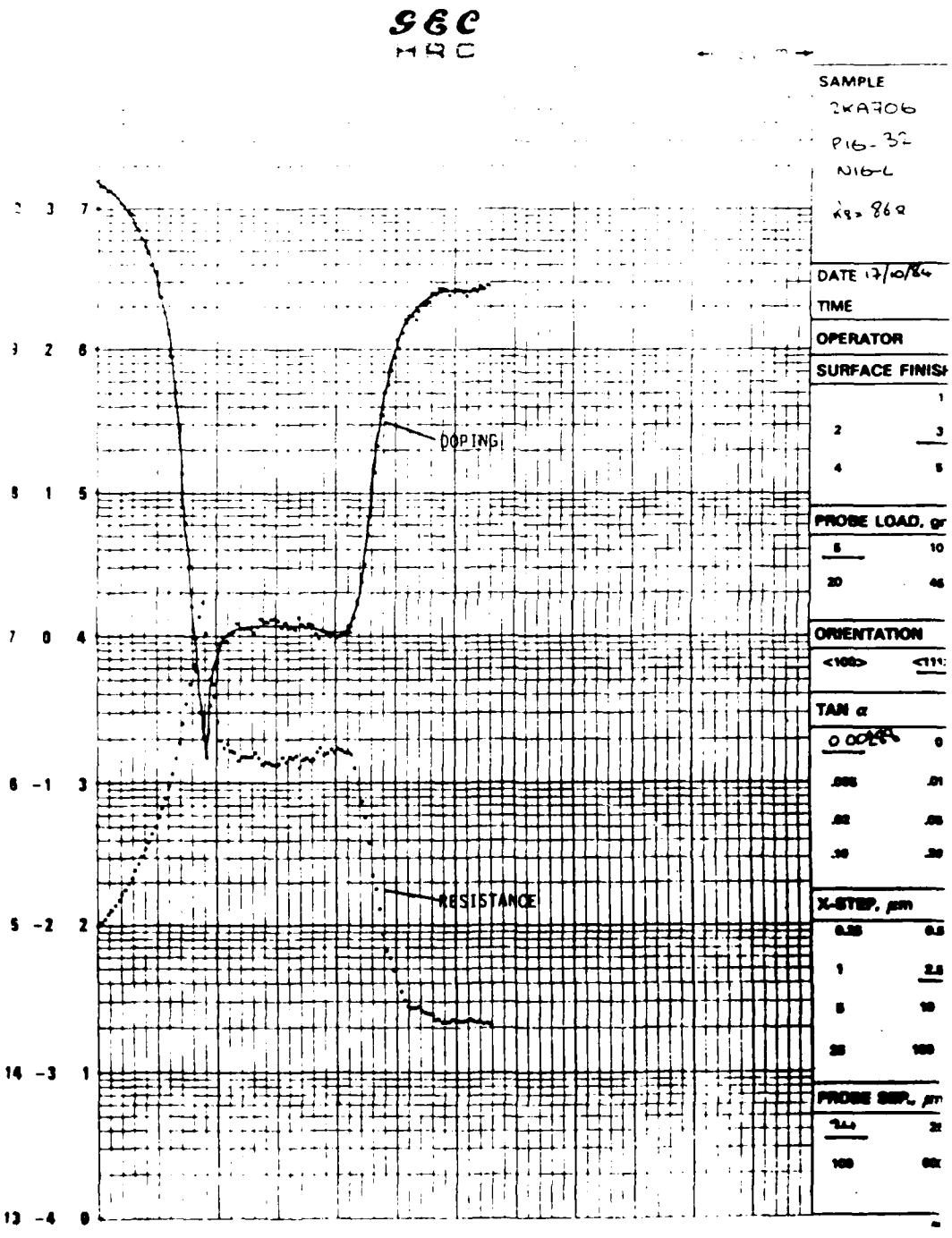

Figure 5.1 : Measured doping profile of W-band IMPATT material.

Figure 5.2 : Modelled doping profile of W-band IMPATT material.

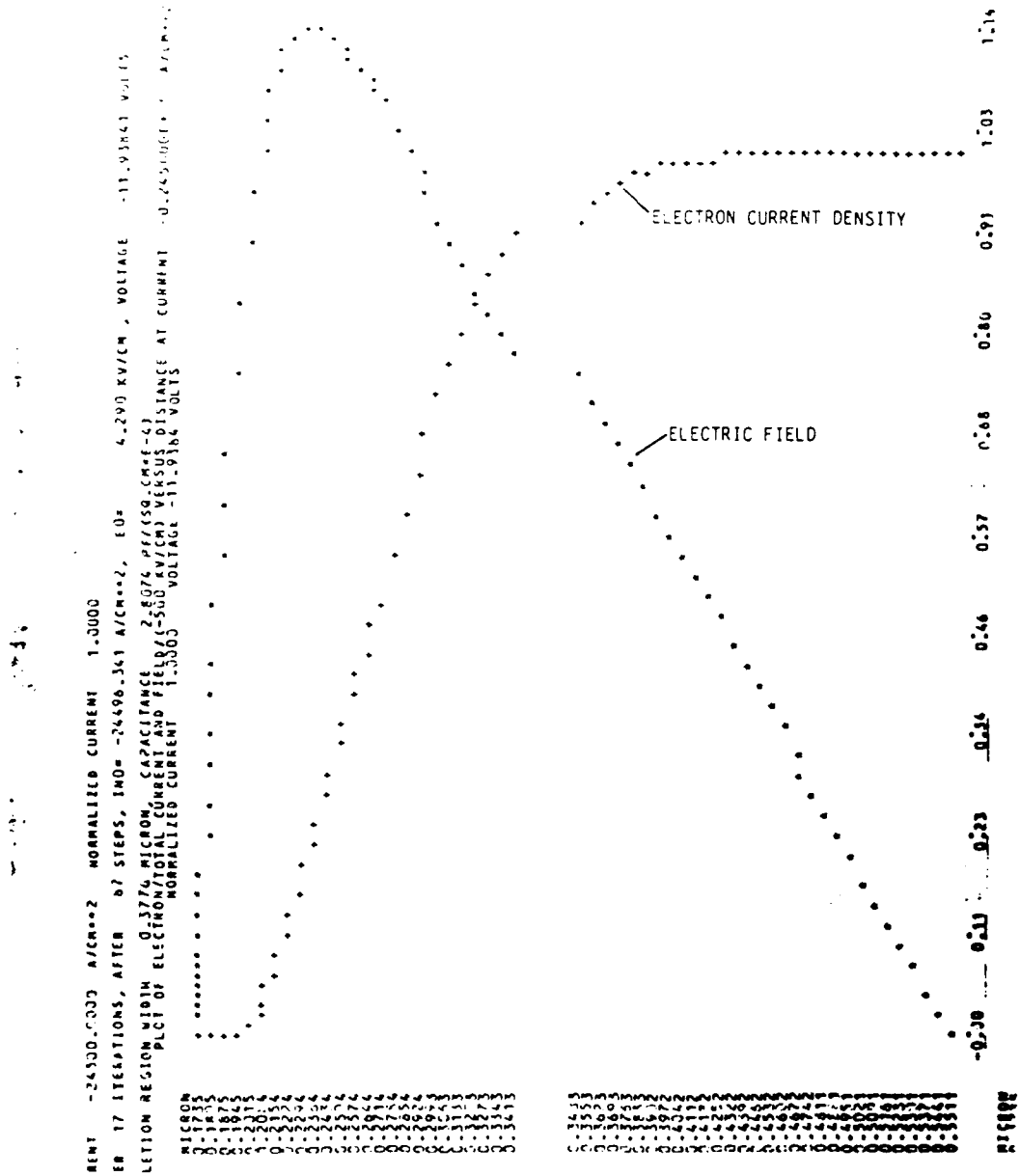

Figure 5.3 : Electric field and electron current density profiles from DCP.

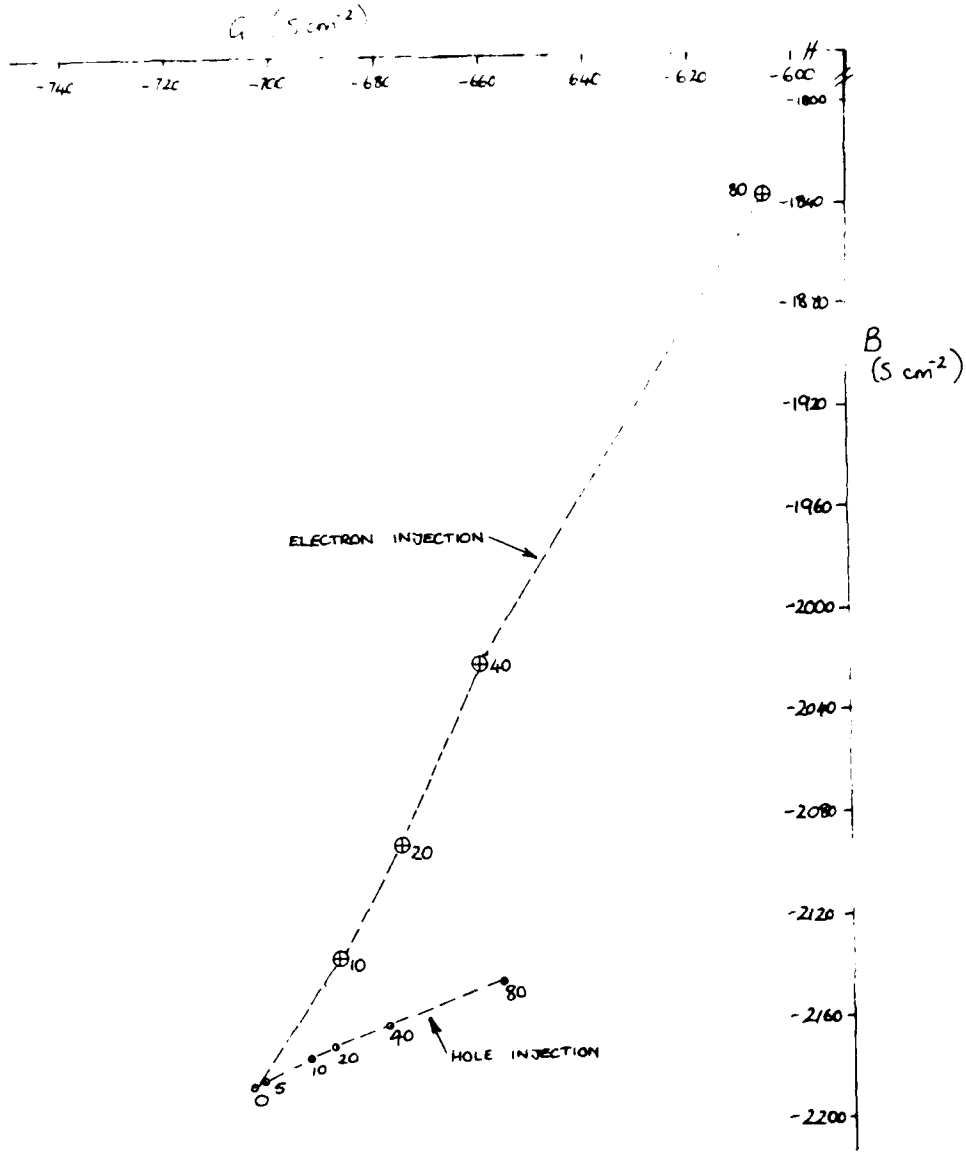

Figure 5.4 : IMPATT diode small signal admittance at 94GHz
parameter : injected minority carrier current density
(Acm^{-2})

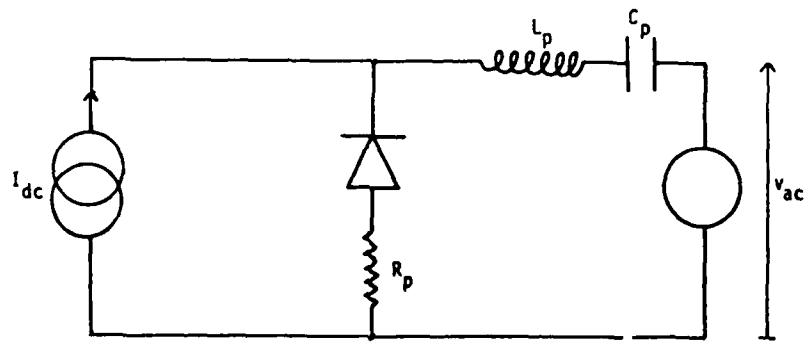

Figure 5.5 : FSP:- voltage control circuit.

```
FREQUENCY AVERAGED OVER     15 CYCLES= 93.945056 GHZ
 FOURIER ANALYSIS FOR FUND FREQ.    94.00000 GHZ FROM TIMESTEP  1861

                      REAL          IMAGINARY        MAGNITUDE
HARMONIC  0

VOLTAGE       =    -0.12243E+02
CURRENT       =    -0.24469E+05
IMPEDANCE     =     0.50020E-03
ADMITTANCE    =     0.19992E+04
DIODE POWER   =    -0.29955E+06
EFFICIENCY    =    -0.99875E+00                                  SAMPLING ERROR =     0.12498E-02
HARMONIC  1

VOLTAGE       =    -0.16645E+01     0.24552E+01     0.29661E+01
CURRENT       =    -0.22048E+05     0.62672E+04     0.22910E+05
IMPEDANCE     =    -0.40794E-04    -0.12287E-03     0.12946E-03
ADMITTANCE    =    -0.24339E+04     0.73307E+04     0.77242E+04
DIODE POWER   =    -0.10706E+05    -0.32246E+05
EFFICIENCY    =     0.35702E-01     0.10753E+00
HARMONIC  2

VOLTAGE       =     0.13282E-02     0.45286E-02     0.47194E-02
CURRENT       =     0.22996E+04     0.12094E+05     0.12311E+05
IMPEDANCE     =     0.36152E-06    -0.37267E-07     0.36334E-06
ADMITTANCE    =     0.25963E+07     0.75360E+06     0.26067E+07
DIODE POWER   =     0.26913E+02    -0.26242E+01
EFFICIENCY    =    -0.96418E-04     0.94180E-05

END OF LISTING OF FILE :UGSE299.SOURCE(1,*,1).FSPOUT(1) FOR USER :UGSE299 AT 1985/05/15__19:28:15
```

Figure 5.6 : FSP:- Result of Fourier analysis of diode terminal current and voltage waveforms.

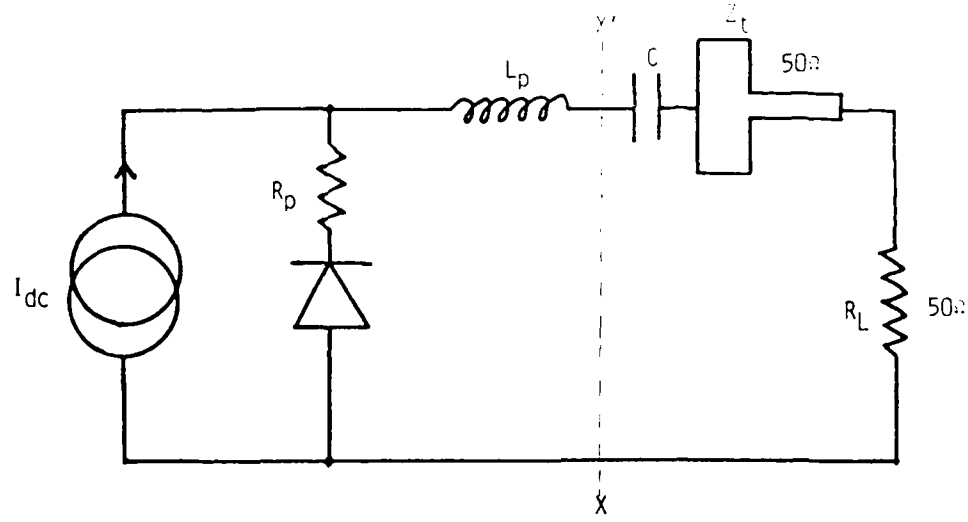

Figure 5.7 : Equivalent circuit for IMPATT oscillator optical tuning experiments.

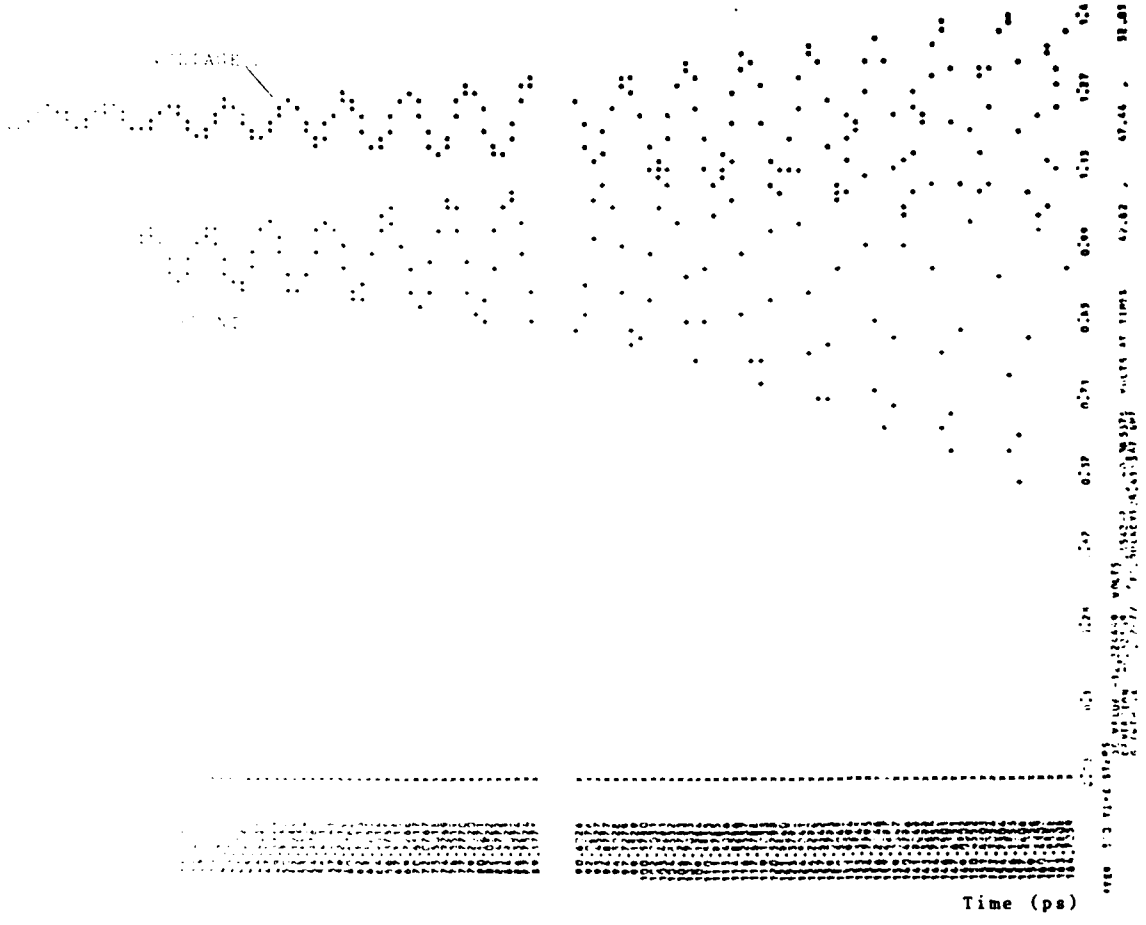

Figure 5.8 : IMPATT oscillator model - build-up of oscillation.

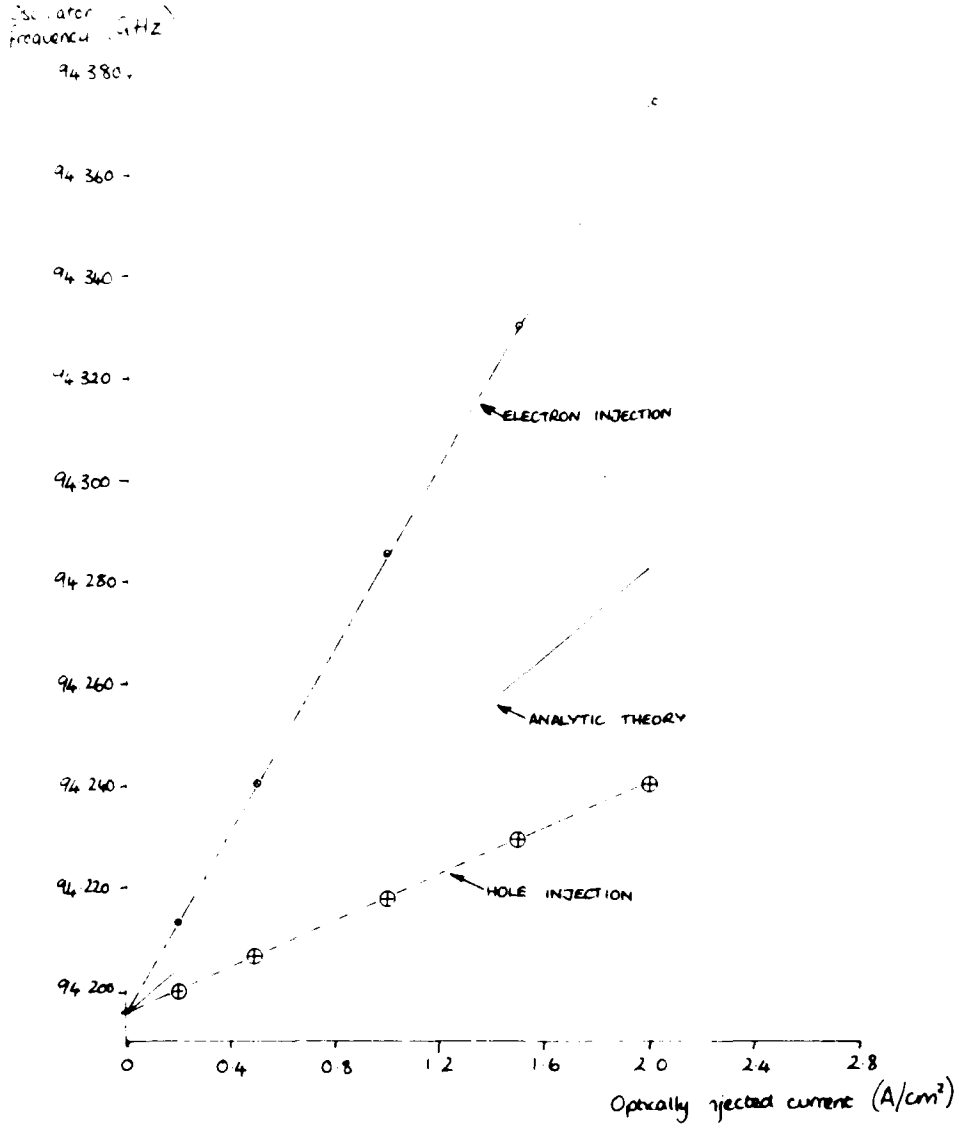

Figure 5.9 : IMPATT oscillator optical tuning characteristics, I_{dc} = 28,450A/cm².

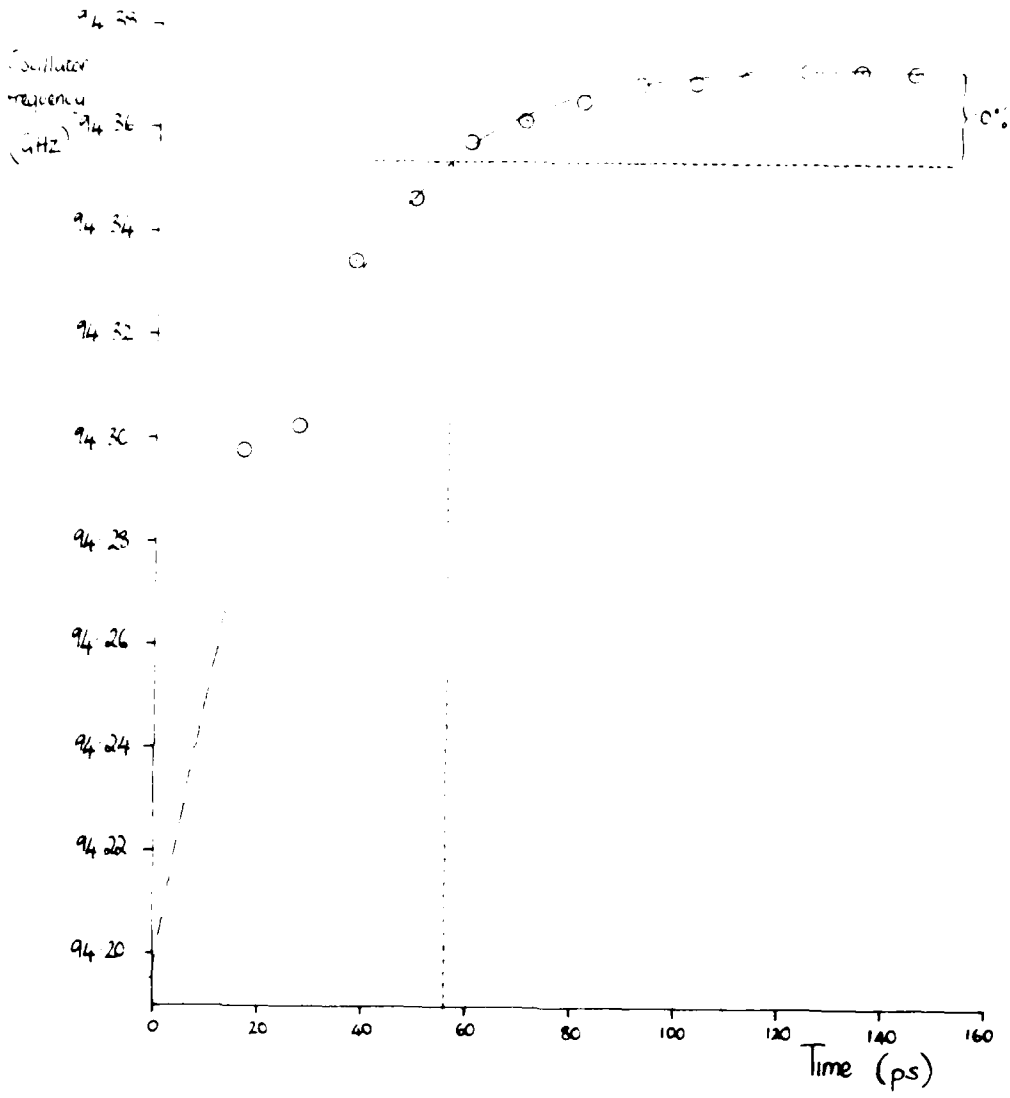

Figure 5.10 : IMPATT oscillator optical tuning transient for step change in illumination, I_p = 0 to 2A/cm², I_{dc} = 28,450 A/cm², electron injection.

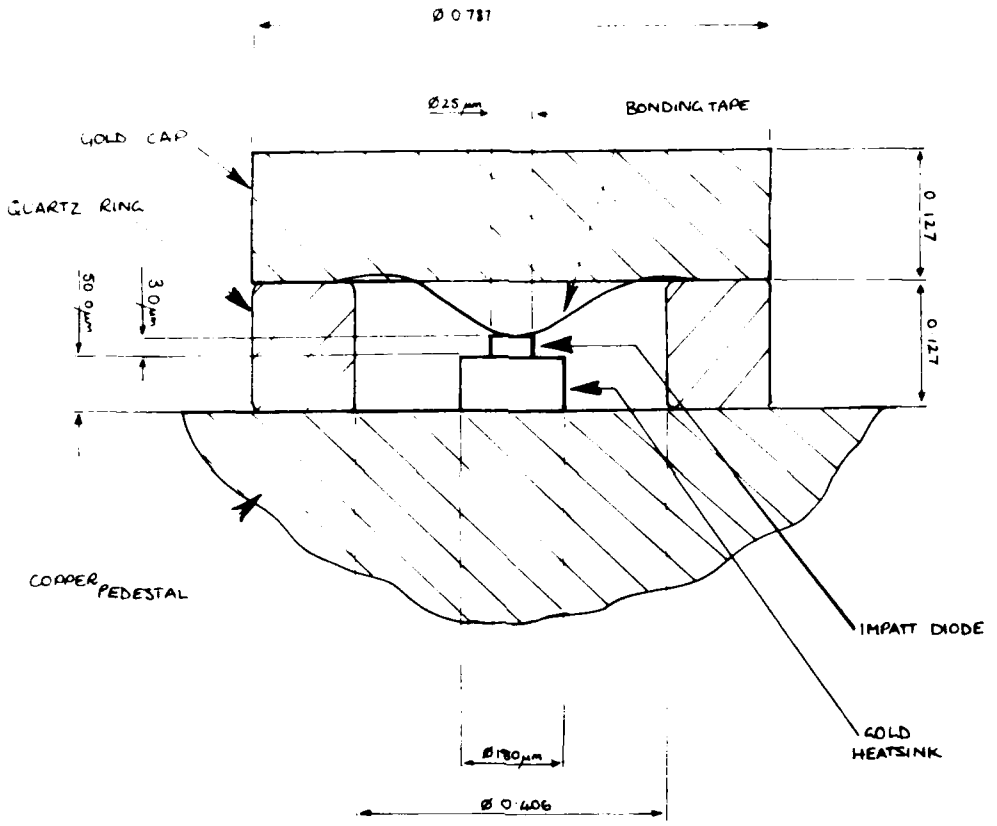

Figure 6.1 : IMPATT diode in quartz ring package.

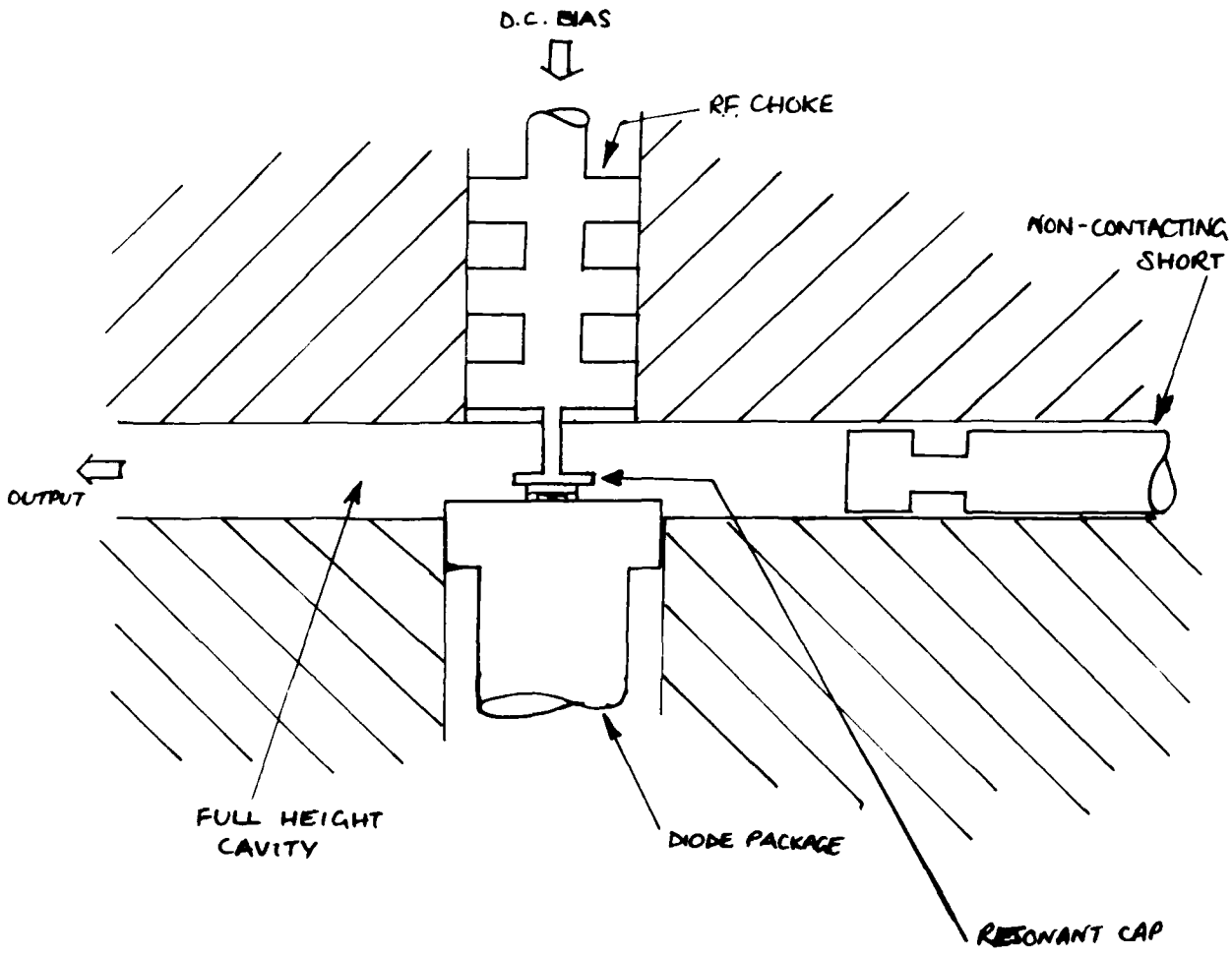

Figure 6.2 : IMPATT oscillator cavity.

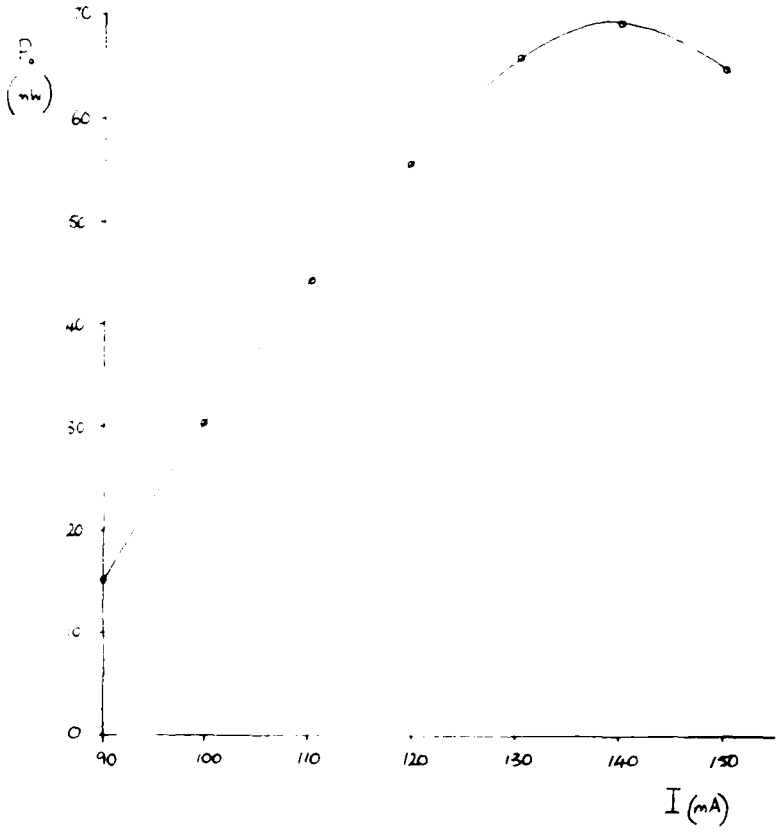

Figure 6.3 : IMPATT oscillator output power vs. bias current at T_{osc} = 33°C.

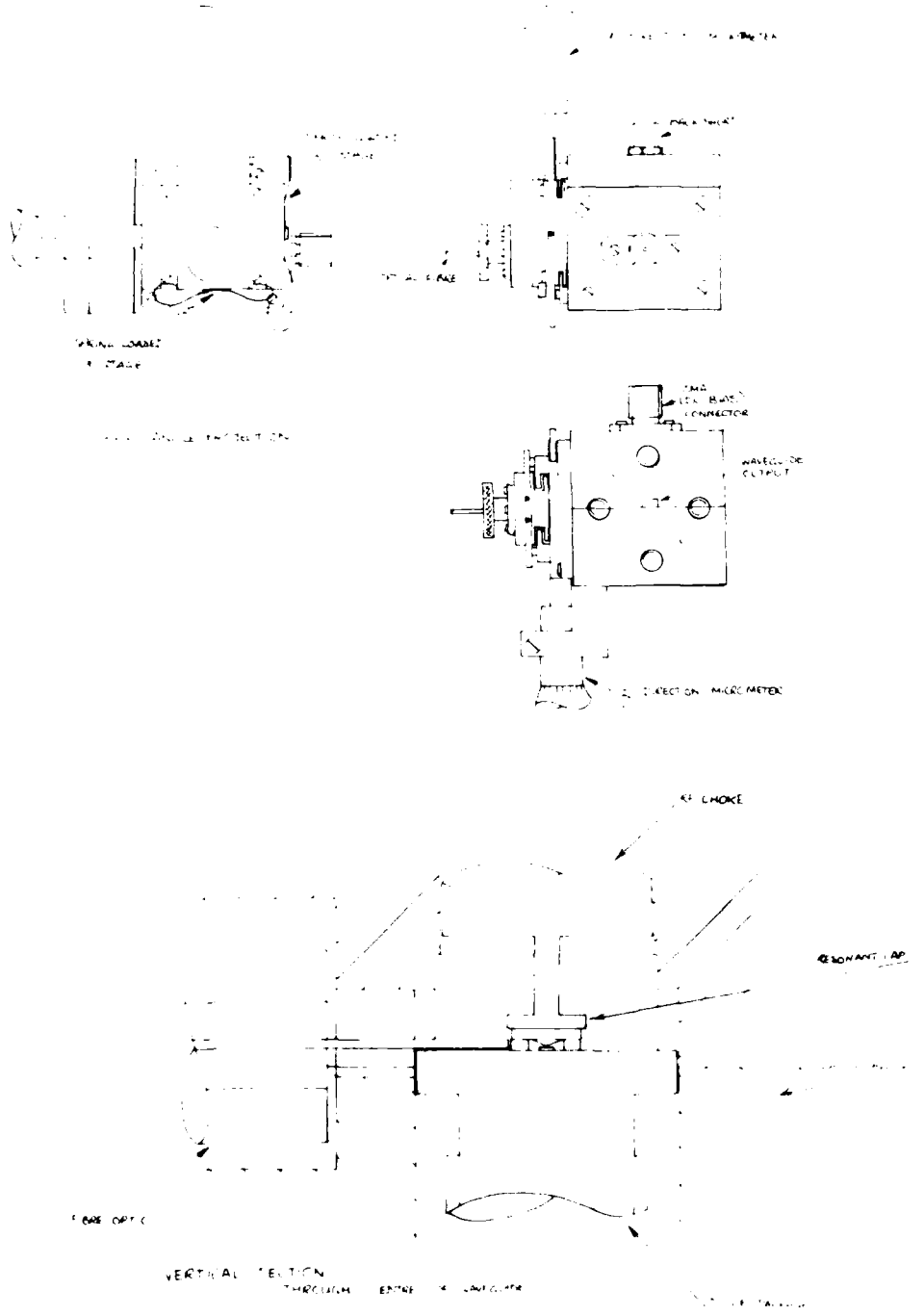

Figure 6.4 : IMPATT oscillator with x-z translational stages.

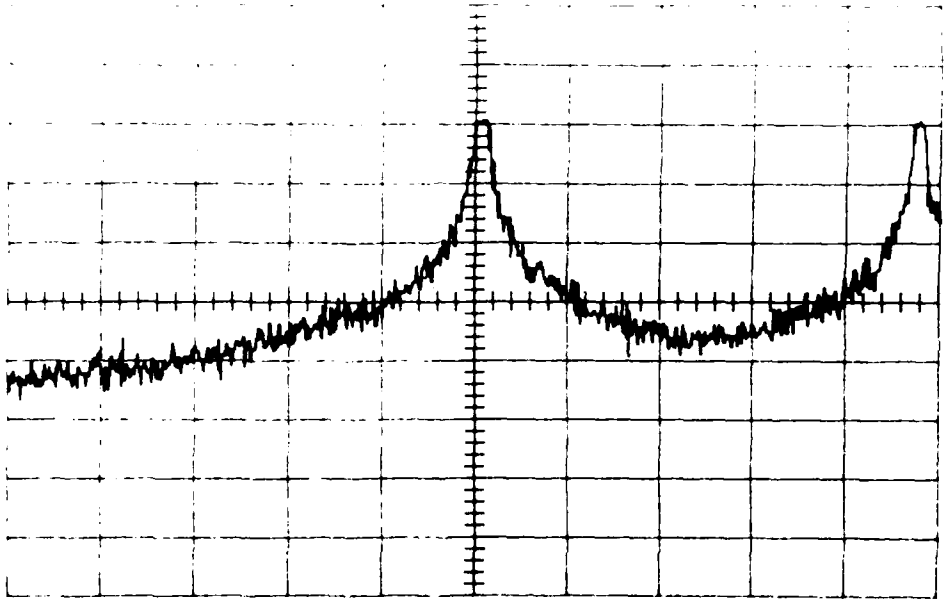

Figure 6.5 : Optical tuning of 9.40MHz at a centre frequency of 91.8268GHz.
Frequency span = 20MHz.
Optically generated current, Iopt = 20.3μa.

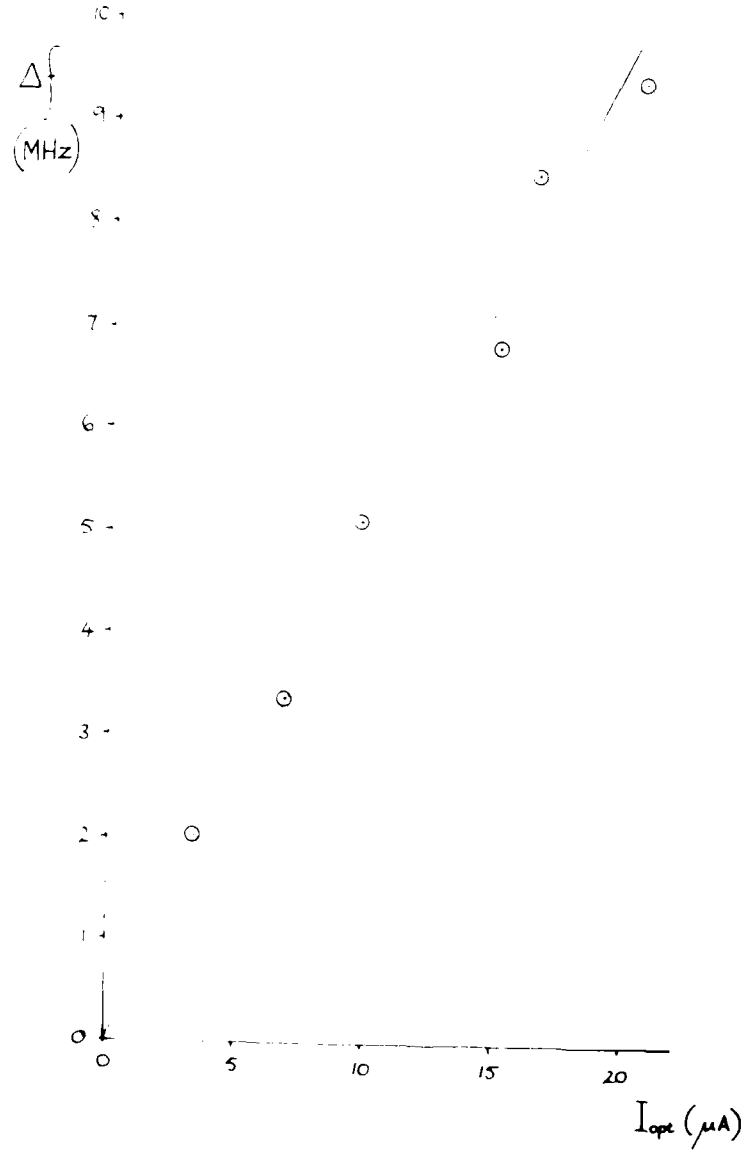

Figure 6.6 : Frequency tuning vs. optically generated current.

DIODE S/N	BIAS CURRENT mA	CENTRE FREQUENCY GHz	OUTPUT POWER mW
222	92	90.3	3.5
209	100	91.7	9.2
212	120	94.4	16.7
213	127	94.5	7.3
224	100	96.1	3.2
203	120	93.8	4.4
215	100	91.9	2.2
225	120	95.7	8.4

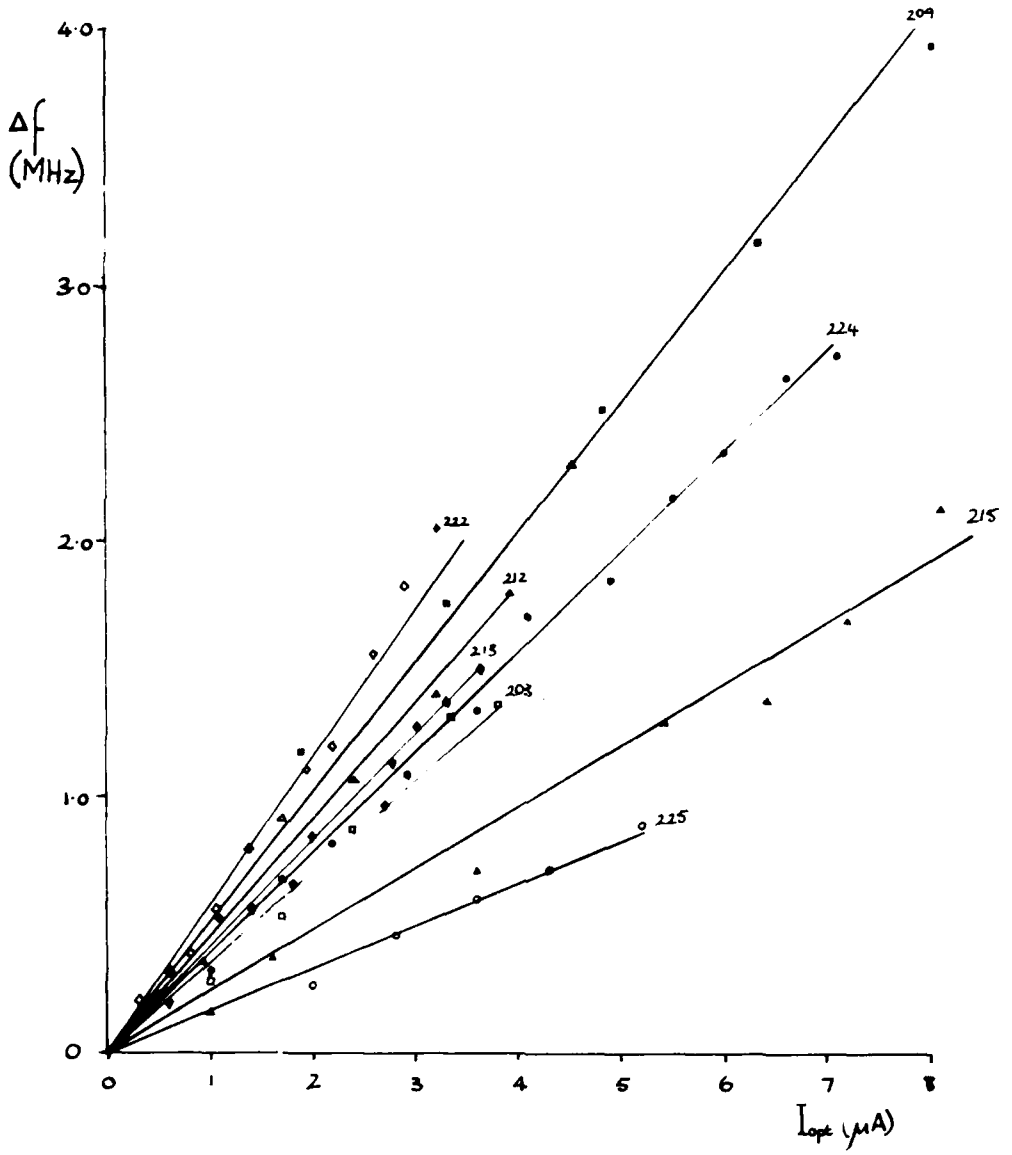

Figure 6.7 : Frequency tuning vs. optically generated current.

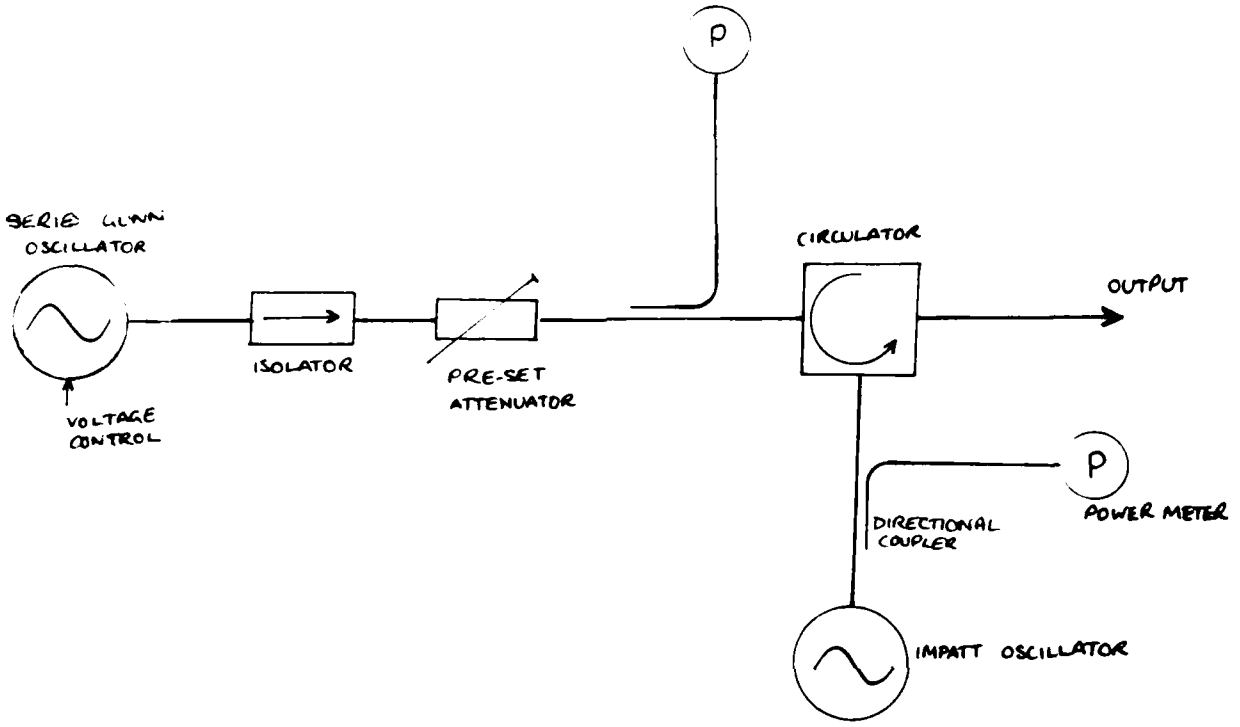

Figure 6.8 : Diagram of injection locking experimental arrangement.

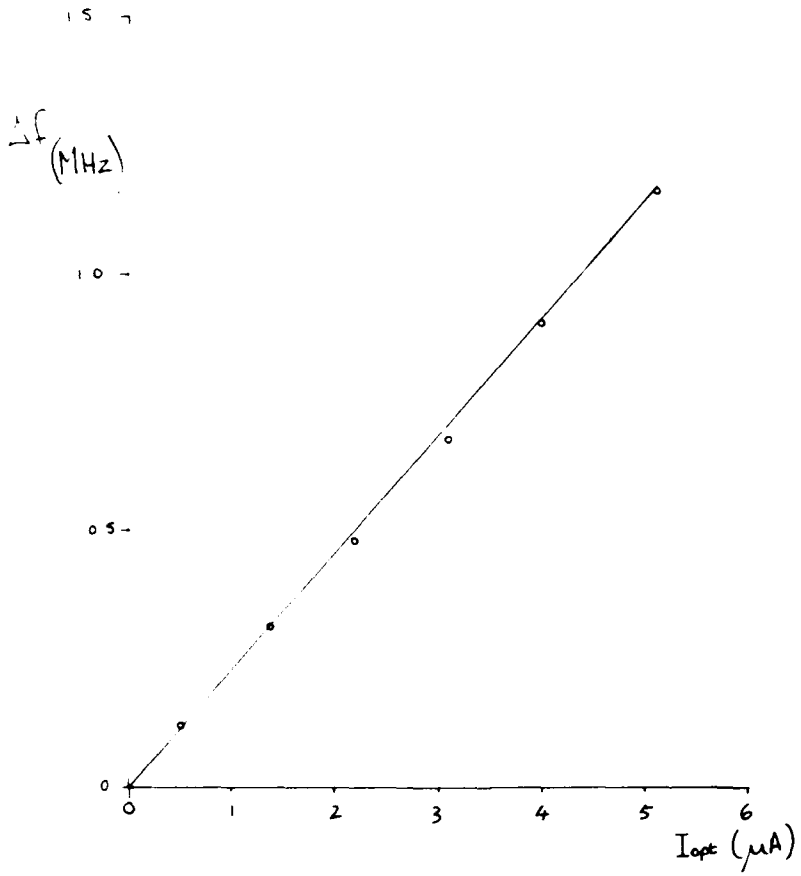

Figure 6.9 : Frequency tuning vs. optically generated current.

APPENDIX 1

Analysis of Oscillator Q Measurement by Injection Locking

Consider the circuit of Figure A1.1

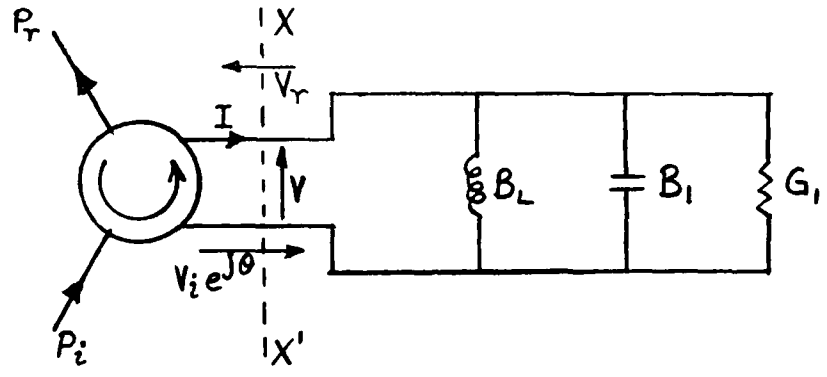

Figure A1.1 Injection locking circuit arrangement.

The equivalent circuit values are normalised to the characteristic admittance of the circulator and transmission line system, G_o. An injected locking signal, P_i, differs in phase from the oscillator output, P_r, by a phase angle θ.

At the plane X-X'

$$V = V_r + V_i e^{j\theta} \qquad \text{.....A1.1}$$

$$I = G_o (V_i e^{j\theta} - V_r) \qquad \text{.....A1.2}$$

Hence the oscillator admittance is given by

$$Y = \frac{G_o (V_i e^{j\theta} - V_r)}{V_r + V_i e^{j\theta}} = G_1 + j (B_1 + B_L) \qquad \text{.....A1.3}$$

If the oscillator capacitance is C and the inductance is L, and if the operating frequency is ω, then separating the admittance into real and imaginary parts yields

$$G_o \left(\frac{V_i^2 - V_r^2}{V_i^2 + V_r^2 + 2V_i V_r \cos\theta} \right) = G_1 \qquad \text{.....A1.4}$$

$$G_o \left(\frac{2 V_i V_r \sin\theta}{V_i^2 + V_r^2 + 2V_i V_r \cos\theta} \right) = \left(\omega C - \frac{1}{\omega L}\right) \qquad \text{.....A1.5}$$

For the free-running case $V_i = 0$ and $\omega = \omega_o$ giving

$$G_o = G_1 \qquad \text{.....A1.6}$$

and

$$\omega_o = \frac{1}{\sqrt{LC}} \qquad \text{.....A1.7}$$

For the case of low level injection $V_i << V_r$ and $\omega = \omega_o + \Delta\omega$, where $\Delta\omega << \omega_o$. Equation A1.5 then reduces to

$$\Delta\omega = \frac{G_o V_i}{C V_r} \sin\theta \qquad \text{.....A1.8}$$

The limits of the locking range are reached for $\theta = \pm \frac{\pi}{2}$. Defining the oscillator Q as

$$Q = \frac{\omega_o C}{G_o} \qquad \text{.....A1.9}$$

gives the total locking range as

$$2\Delta\omega_\ell = \frac{2\omega_o}{Q} \frac{V_i}{V_r} \qquad \text{.....A1.10}$$

which can be re-expressed in terms of power as

$$2\Delta\omega_\ell = \frac{2\ \omega_o}{Q} \sqrt{\frac{P_i}{P_r}} \qquad \text{.....A1.11}$$

The oscillator Q can therefore be found by measuring the locking range for low level injection and substituting in the equation

$$Q = \frac{2\omega_o}{2\Delta\omega_\ell} \sqrt{\frac{P_i}{P_r}} \qquad \text{.....A1.12}$$

OPTICAL CONTROL OF W-BAND IMPATT OSCILLATORS

J. F. Singleton, A. J Seeds and S. P. Brunt

Abstract

The paper presents the results of analytical, computer modelling and experimental studies of optically induced frequency tuning in a W-Band (95 GHz) IMPATT oscillator. Predictions from an analytic theory are compared with those from a large signal time-domain computer model, and the effect of unequal electron and hole ionisation coefficients on the tuning performance illustrated. Experimental measurements, showing an optical tuning range of about 10 MHz for an optically generated current of 20 μA, are given and compared with the theoretical predictions.

1. Introduction

The IMPATT diode continues to be an important power source at millimetre wavelengths. However it is difficult to tune the oscillation frequency electronically because of the power and impedance levels involved. A promising technique is the use of an optical signal to generate carriers in the IMPATT by the photo-electric effect. These carriers drift into the avalanche zone of the diode and alter the phasing of the avalanche cycle, thereby changing the oscillation frequency.

Optical frequency tuning effects have previously been observed in TRAPATTs [1], bipolar transistors [2] and MESFETs [3]. Early work on the optical tuning of IMPATTs was mostly carried out at X-Band [4,5]. This paper reports work to extend the technique to W-Band.

2. Analytic Theory of Optical Frequency Tuning in IMPATT Oscillators

The physical mechanism underlying optical frequency tuning is the generation of hole-electron pairs in the IMPATT by the incident light, with consequent alteration in the timing of the avalanche cycle. It is therefore possible to calculate the change in oscillation frequency using a modified Read [6] approach. Making the simplifying assumptions of equal carrier velocities and avalanche ionisation coefficients for holes and electrons, the total avalanche current is given by [5]

$$\frac{\tau_a}{2}\frac{dJ}{dt} = J\left[\int_0^{W_a} \alpha\, dz - 1\right] + J_s \qquad \text{--- 2.1}$$

where J_s is the total reverse saturation current density including both thermal and optical carrier generation, α the avalanche ionisation coefficient, W_a the

---

J. F. Singleton and S. P. Brunt are with Marconi Electronic Devices Ltd., Doddington Road, Lincoln, LN6 3LF.
A. J. Seeds is with the Department of Electrical and Electronic Engineering, Queen Mary College, Mile End Road, London, E1 4NS.

avalanche zone width and τ_a the avalanche zone transit time. Integration of equation 2.1, using a power law approximation for the dependence of the ionisation coefficient on electric field together with a transit time model for the drift zone, enables the change in oscillator frequency with optically injected current to be written

$$\Delta f_o = \frac{I_{so} \, (2 \, I_0^2\{X\} - 3 \, I_0\{X\} \, I_2\{X\})}{4 \, \pi \, Q \, I_{dc} \, \tau_a} \qquad \text{--- 2.2}$$

where I_{so} is the mean optically generated current, I_{dc} the diode bias current, Q the oscillator external Q factor, and $I_n\{X\}$ are modified Bessel functions of argument

$$X = \frac{(m + 1) \, V_1}{\pi \, f_o \, \tau_a \, E_{po} \, w} \qquad \text{--- 2.3}$$

where f_o is the oscillation frequency, V_1 the peak r.f. voltage across the diode, E_{po} the peak electric field at breakdown, w the total depletion width and m the ionisation non-linearity coefficient. In equation 2.2 the bracketed term arises from the avalanche multiplication of optically generated carriers; this increases sharply with increasing voltage swing through the V_1 dependence of the Bessel function argument, X.

The relationship between the optically generated current and the incident optical power is dependent on the device structure and illumination geometry. Assuming that all of the light is absorbed within the depletion layer the optically generated current is given by

$$I_{so} = \frac{\eta_q \, e \, \lambda \, P_{op}}{h \, c} \qquad \text{---2.4}$$

where P_{op} is the incident optical power, η_q the quantum efficiency, λ the optical wavelength, e the electronic charge, h Planck's constant and c the velocity of light in vacuo. For λ = 850 nm and η_q = 0.9 I_{so}/P_{op} = 0.62 A W^{-1}. In practice difficulties in securing efficient coupling between the light source and the IMPATT lead to much smaller values.

3. Computer Modelling Studies

The analytical theory, whilst useful for estimating the magnitude of optical tuning effects, is limited in accuracy by the equal ionisation coefficients assumption, and in any case cannot be used to study transient effects. A large signal time-domain computer model of the optically controlled IMPATT has therefore been developed from the earlier avalanche diode modelling work of Blakey et al [7]. The model is based on the solution in one spatial dimension and time of the approximate form of Boltzmann's transport equation, the equations for electron and hole continuity and Gauss's theorem, within the semiconductor material of the device. This approach enables spatially varying optical carrier generation to be taken into account.

Modelling studies were performed for a W-Band, silicon, single drift structure having a doping profile similar to that of the devices used in the experimental work. A simplified oscillator equivalent circuit, shown in Figure 1,

was applied to the diode to permit predictions of optical frequency tuning. With a bias current of 140 mA the oscillation stabilised at a frequency of 94.195 GHz with 23% voltage modulation.

Two optical carrier generation configurations were investigated. In the first, electrons were injected into the depletion zone from the P^+ region whereas in the second holes were injected from the N^+ region. These correspond to illumination from opposite ends of the IMPATT structure. Figure 2 shows the optical tuning characteristics obtained for optically injected current densities of up to 2 A cm^{-2}, corresponding to a current of 10 μA in the experimental diode. The change in frequency with injected current is seen to be linear, as predicted by equation 2.2. A more detailed comparison with the analytic theory can be made by substituting appropriate values into equations 2.2 and 2.3. For $m = 6$, $\tau_a = 0.1\ f_o^{-1}$, and $Q = 1.6$, with the modelled bias current and voltage modulation, $\Delta f_o / I_{so} = 8.8$ MHz μA^{-1}. This slope is plotted as a broken line in Figure 2. The modelled values for electron and hole tuning lie above and below this line respectively. This is because the analytic theory assumes equal avalanche ionisation coefficients for electrons and holes whereas in silicon those for electrons are much greater than those for holes. Thus electron injection produces a much greater tuning effect than hole injection. With this restriction, agreement between the analytic theory and the modelling results is seen to be good.

4. Experimental Work

The IMPATT diode used was mounted in a quartz ring package and placed in a resonant cap type waveguide oscillator circuit, as shown in Figure 3. A GaAs/GaAlAs laser, emitting at a wavelength of 850 nm, was used as the optical source. Light was coupled to the IMPATT through a 50/125 μm optical fibre, with the coupling optimised using a micromanipulator.

The maximum optically injected current obtained was 21 μA for an optical power, measured at the fibre end of 3 mW. From equation 2.4 this power should be sufficient to generate a current of about 1.9 mA. The low coupling efficiency is due partly to refraction in the quartz ring package and partly to the small height of the IMPATT structure (≈ 3 μm total) relative to the fibre core diameter of 50 μm.

Figure 4 shows the change in oscillator frequency with optically injected current, for a bias current of 100 mA, which gave an output power of 9 mW at a frequency of 91.8 GHz. As expected the frequency shift is proportional to injected current. The tuning slope is approximately 0.5 MHz μA^{-1}. This value is considerably smaller than those for the computer modelling work due to the much higher Q factor of the experimental oscillator circuit (measured Q = 160). From the measured output power the voltage modulation was estimated at 22%, giving a tuning slope of 0.24 MHz μA^{-1} from equation 2.2. The measured value is just within the range of variation possible due to the composition of the optically generated current (see Figure 2). However, the illumination geometry used would be expected to lead to significant hole current generation: further investigation is therefore required.

5. Discussion

Optical frequency tuning of a W-Band IMPATT oscillator has been demonstrated. The measured tuning range of about 10 MHz is within a factor of two of that predicted theoretically. Further investigation is being carried out into the causes of the discrepancy. The tuning range could be greatly increased if

the coupling of the light to the IMPATT structure were improved. Assuming that linearity of the tuning characteristic was maintained a tuning range of 950 MHz should be possible with the present laser source. Methods of improving the coupling include the replacement of the quartz ring package with one using quartz stand-offs, the formation of a lens on the end of the optical fibre, the use of mirrors to concentrate the incident light and the fabrication of special IMPATT structures intended to facilitate illumination of the active area. Several of these possibilities are currently under investigation.

Further work on the computer model will be directed towards developing an equivalent circuit for the experimental oscillator design so that detailed comparisons between the predictions of the model and measured results can be made.

Optical tuning provides a technique for controlling the frequency of IMPATT oscillators which offers electrical isolation and ease of control signal distribution through optical fibres. It is envisaged that, following further development, the technique will prove useful in a number of millimetre-wave radar and communication system applications.

6. Acknowledgements

The authors are grateful to Dr. J. R. Forrest (Marconi Defence Systems, Stanmore) for useful discussions. This work was supported by the United States Army under contract DAJA45-84-C-0045.

7. References

1) Kiehl, R. A. and Eernisse, E. P.:'Control of TRAPATT oscillations by optically generated carriers', IEEE Trans., 1977, ED-24, pp. 275-277.

2) Yen, H. W. and Barnoski, M. K.:'Optical injection locking and switching of transistor oscillators', Appl. Phys. Lett., 1978, 32, pp. 182-184.

3) Salles, A. A.:'Optical control of GaAs MESFETs', IEEE Trans., 1983, MTT-31, pp. 812-820.

4) Vyas, H. P., Gutmann, R. J. and Borrego, J. M.:'Optical-microwave effects in IMPATT diode oscillators', IEEE MTT Symp. Tech. Digest, 1979, pp. 188-190.

5) Forrest, J. R. and Seeds, A. J.:'Analysis of the optically controlled IMPATT (OPCAD) oscillator', IEE J. Solid-State and Electron Devices, 1979, 3, pp. 161-169.

6) Read, W. T.:'A proposed high-frequency negative-resistance diode', Bell Syst. Tech. J., 1958, 37, pp. 401-446.

7) Blakey, P. A., Giblin, R. A. and Seeds, A. J.:'Large-signal time-domain modelling of avalanche diodes', Trans. IEEE, 1979, ED-26, pp. 1718-1728.

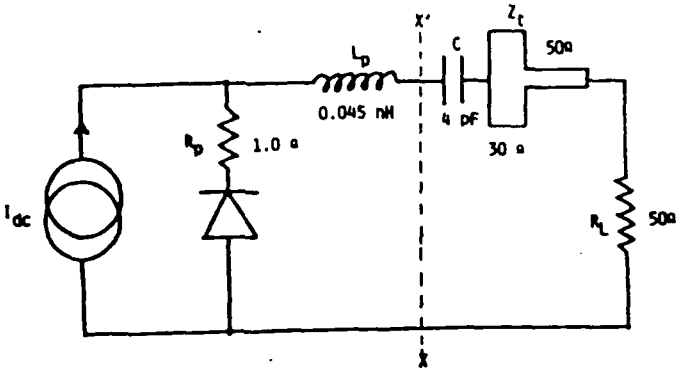

Figure 1.: Oscillator equivalent circuit for modelling studies.

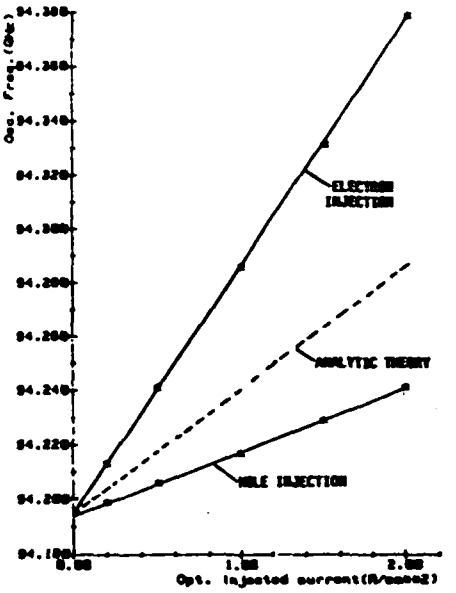

Figure 2.: Comparison between computer model and analytic theory for optical tuning characteristics. (Bias current density 28.5 kA cm^{-2}.)

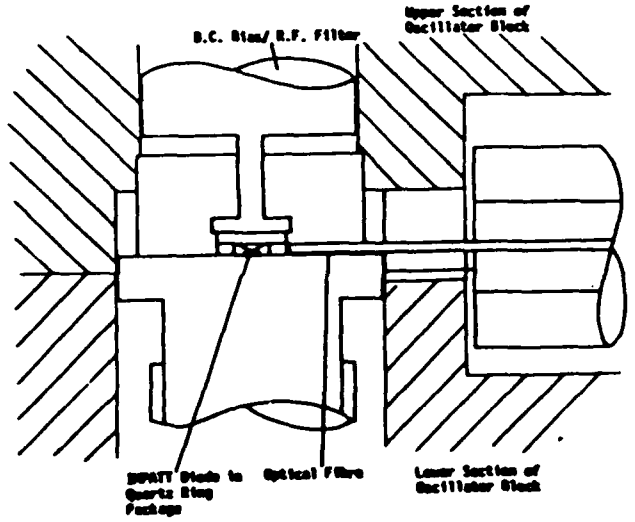

Figure 3.: Experimental W-Band optically controlled IMPATT oscillator.

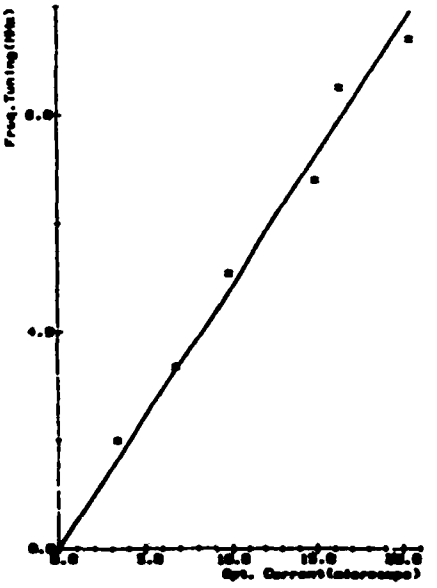

Figure 4.: Measured optical tuning characteristic.

END

2-87

DTIC